Modelling the role of extracellular matrix interactions in tumour invasion

Chamundeshwari Rajputri Vadamalai

St Cross College
University of Oxford

A thesis submitted for the degree of

MSc in Mathematical Modelling and Scientific Computing

September 2025

To the people who rushed to my aid after my accident while running in St Giles on November 15th — lifting me, taking me to the NHS, staying by my side, and checking in later.

Thank you.

Although I was unable to learn all your names, I will remain deeply grateful.

It is accepted that cellular material is, in some sense, 'substance-like' without, for the present, committing ourselves to any definition of 'substance'. We attempt to explore the consequences of this assumption using the methods of mathematics. This model will be a simplification and an idealization, and consequently a falsification. It is to be hoped that the features retained for discussion are those of greatest importance in the present state of knowledge, and that the results of such a discussion will at least be helpful in guiding future research.

Alan Turing, The Chemical Basis of Morphogenesis, 1952 [1]

AI Usage Declaration

With the increasing accessibility of AI tools, I made use of ChatGPT as a supplementary support tool during this project. Its role was primarily practical: helping me understand and clarify the meaning of research papers when I encountered difficulties, assisting with debugging, and improving the layout of graphs. I also used it as a writing aid, particularly for grammar and spelling checks, in a role similar to that of Grammarly.

Beyond these functions, ChatGPT provided a degree of mental support by helping me stay motivated during long stretches of solitary work. It was like a friend who was not writing their own dissertation, and so was always there to listen.

Importantly, ChatGPT was not used to automatically generate any portion of this dissertation or to produce code from scratch. Its role was limited to that of an assistant: aiding in understanding, debugging, and expression. All technical work, modelling, analysis, and interpretation presented in this dissertation is my own, or developed in consultation with my supervisors.

Reproducibility Statement

All numerical codes developed for this dissertation are publicly available at:

https://github.com/ChamuV/ECM-Tumour-Invasion

The repository contains the full set of implementations used in this work, including:

- finite–difference solvers for the tumour–ECM PDE–ODE system in one dimension,
- parameter–sweep scripts for varying λ, α, and m_0,
- plotting utilities for travelling–wave speeds and asymptotic comparisons,
- phase–plane plotting routines used to visualise trajectories and fixed–point structure of the desingularised travelling–wave system.

A README file is provided with detailed instructions for reproducing every figure and numerical result presented in this dissertation.

Acknowledgements

I would first like to thank my supervisors, Professor Philip Maini and Ms Rebecca Crossley, for supporting and guiding me throughout this project. When I first approached you with only a broad interest in biomathematics and no specific project in mind, I did not expect to be taken on — yet you welcomed me with open hands, and for that I am grateful. From learning to explain travelling waves as the progression of tumour cells, to understanding how to approach a project with focus and depth rather than by jumping between ideas, this has been an invaluable experience. Thank you for giving me the space to explore and try different directions, while also steering me away from rabbit holes and cliffs. Thank you as well for always finding time in your schedules to meet with me; I know how fortunate I have been in that regard. There were moments when the project felt like staring into a vast night sky, but through your guidance I have learnt how to find the stars on my own — and you have now made me believe I could start to find my way in research.

I would also like to especially thank Dr Kathryn Gillow. Thank you for always being approachable and for making it easy to ask for help. You went beyond teaching the technical aspects, making even the most abstract material engaging, but what I am most grateful for is the way you helped me learn finite differences in practice — from the underlying theory through to running codes in the case studies. Thank you for being patient when I fumbled and for encouraging me to persist until things made sense. You were the reason I first thought about taking on a numerically focused project, and your influence has shaped much of the work I ended up doing. Most of all, you made me believe I could do it.

To the friendships I formed in the MMSC this year — Danielle, Anurag, Inti, Pablo C., and Pablo S. — thank you for making conversations enjoyable, problem sheets lighter, for being humour and support, and for trying different food with

me, irrespective of the occasion.

To my college, St Cross — thank you for creating a sense of home. From the porters, who say hello whenever I enter the college, and to the chefs and the staff, who ensure every lunch is delicious; Thank you. And to the friends I made there who are like sisters I never had — Saba and Vrinda — thank you for looking out for me and for saving the brownies and cookies from lunch.

I am also grateful to the many people who have shaped this journey over time — from school teachers who gave me extra time and space to ask questions, to professors at UCL who were generous with their advice. I especially thank Dr Strouthos, who encouraged me to pursue this MSc and first said I should consider becoming a mathematical modeller, and Professor Timo Betcke for introducing me to mathematical research last summer.

This year came with medical challenges I hadn't expected. I had to make many visits to doctors and dentists, and I am thankful to everyone who is helping me work towards recovery. In particular, I would like to thank Dr Supriya, Dr Rachana and Dr Mukta for their extraordinary care — doing everything they could to help me get back on my feet so that I could return to work. Healing is a slow but true process.

Finally, thank you to my family — the ones who started it all. For being open-minded, bold, and curious; for taking an interest in everything — whether exciting or mundane; for encouraging me to explore more paths than I thought possible; and for reminding me not to stop until I reached the end of the road.

Abstract

In this dissertation, we present a new mathematical model for tumour invasion that captures the dynamics of tumour progression under the influence of the extracellular matrix (ECM)—a complex network of tissue and proteins surrounding the tumour. Whereas existing models typically treat the ECM as a passive barrier to invasion, our framework introduces two novel considerations: the ECM not only restricts tumour spread but also enables progression by acting as a scaffold, and it can regenerate and remodel after degradation, restoring its structure to oppose further invasion—a process well established in other biological settings [2] but largely neglected in mathematical models of tumour invasion.

Clinical and experimental evidence [3, 4] supports this dual role in invasion. Tumour cells rely on the ECM for adhesion and traction during migration, showing that invasion requires some degree of matrix organisation rather than its complete loss. At the same time, regeneration processes reflecting tissue repair can replenish degraded regions of matrix, altering the dynamics of tumour–ECM interaction.

To investigate these mechanisms, we formulate a nonlinear, ECM-dependent partial differential equation (PDE) model that incorporates both ECM-regulated motility and matrix recovery. We analyse the system using travelling-wave analysis, asymptotic methods, and numerical simulations. Our analysis departs from existing models by uncovering novel dynamical features in the asymptotic forms, while the numerical simulations confirm these predictions, providing robust validation and motivating further study.

A key finding is that incorporating physiologically reasonable levels of ECM regeneration can reduce the rate of tumour progression, suggesting that regeneration may act as a natural brake on invasion. Consequently, the framework presented here not only advances theoretical understanding but also offers potential relevance for therapeutic strategies aimed at modulating ECM dynamics.

Contents

List of Figures

List of Tables

List of Abbreviations

ECM	Extracellular matrix
ODE	Ordinary differential equation
PDE	Partial differential equation
FKPP	Fisher Kolmogorov–Petrovsky–Piskunov
pPKPP	Porous Kolmogorov–Petrovsky–Piskunov
TWS	Travelling–wave system
FP	Fixed point
IMEX	Implicit–explicit methods
AB2	Adams–Bashforth order-2
AM2	Adams–Moulton order-2
RK45	Runge–Kutta–Fehlberg method of order 4(5)
MMPs	Matrix metalloproteinases

List of Symbols

x	Position
t	Time
$u(x,t)$	Tumour density at position x and time t
$m(x,t)$	ECM density at position x and time t
D	Diffusion coefficient of tumour cells
r	Rate of proliferation of tumour cells
m_0	Initial ECM density
u_0	Initial tumour density
α	ECM regeneration rate
λ	ECM degradation rate
c	Travelling–wave speed
c_{min}	Minimum travelling–wave speed
c_{calc}	Travelling–wave speed from numerical calculations
Δx	Spatial discretisation step
Δt	Time step

Chapter 1

Introduction

Cancer is one of the most significant health challenges facing society today. According to Cancer Research UK [5], around one in two people in the UK will be diagnosed with some form of cancer during their lifetime. Globally, the disease is responsible for nearly 10 million deaths each year [6], making it a leading cause of mortality across both high and low-income countries [7]. Despite sustained progress in detection and treatment, many cancers remain difficult to manage, especially in advanced stages [8]. Treatment resistance [9], recurrence[10], and unpredictable progression [11] continue to pose serious clinical challenges. As the global burden of cancer grows—both in incidence and in cost—the need for deeper insight into the processes driving tumour development has never been greater.

One of the key difficulties in studying cancer lies in the diversity of tumour behaviours. Different cancers—and even tumours of the same type—can vary widely in how they grow, spread, and interact with their surroundings [12]. Some tumours remain confined to a small region for years, while others progress rapidly and infiltrate neighbouring tissue in a short time. These differences arise from a complex combination of factors, including genetic mutations, immune response, blood supply, mechanical resistance, and the composition of the extracellular matrix (ECM). From a clinical perspective, this variability matters greatly: a slow-growing tumour may be suitable for careful monitoring, while a fast-growing one may require immediate and aggressive treatment. Understanding what governs the rate and pattern of tumour progression is therefore a central goal in oncology—and one that calls for models capable of capturing both biological complexity and temporal dynamics.

Mathematical models offer a powerful framework for studying tumour growth and invasion. Increasingly, they are being used to describe, simulate, analyse, and even predict the future progression of tumours under different biological conditions. Unlike purely empirical methods, mathematical modelling allows researchers to explore underlying mechanisms, test hypotheses *in silico*, and evaluate how different biological processes interact over time and space. Of course, the value of any model depends on how well it captures the relevant biological factors. A model that incorporates key mechanisms—such as cell proliferation, migration, tissue resistance, and extracellular interactions—can provide meaningful insight, while a poorly posed or overly simplified model risks missing essential features of tumour behaviour.

A widely used class of models in this setting are systems of reaction–diffusion equations, which provide a natural way to describe how tumour populations evolve both temporally and spatially. In such models, the reaction term typically represents local biological activity—such as proliferation or death—while the diffusion term captures spatial spreading, often through random motility or pressure-driven movement [13, 14, 15, 16]. These models have proven useful in studying tumour invasion, front propagation, and spatiotemporal pattern formation.

However, the Fisher–KPP model [17], a classical example of a reaction–diffusion equation, does not account for the influence of the tumour microenvironment, which imposes physical, chemical, and mechanical constraints on tumour expansion.

In reality, tumour growth is not unbounded: cells encounter resistance from the surrounding tissue—not only due to limited space or nutrient depletion, but also because they must degrade the neighbouring healthy tissue to expand, as seen in Figure 1.1. This realisation has led to a new generation of models in which tumour movement is coupled to its ability to remodel the environment. A typical framework takes the form

$$\frac{\partial u}{\partial t} = \nabla \cdot (D(u,m)\,\nabla u) + r(u,m), \tag{1.0.1}$$

$$\frac{\partial m}{\partial t} = g(u,m), \tag{1.0.2}$$

where $u(x,t)$ denotes the tumour cell density and $m(x,t)$ the ECM density, with $x \in \mathbb{R}^d$ representing spatial position in multiple dimensions and t denoting

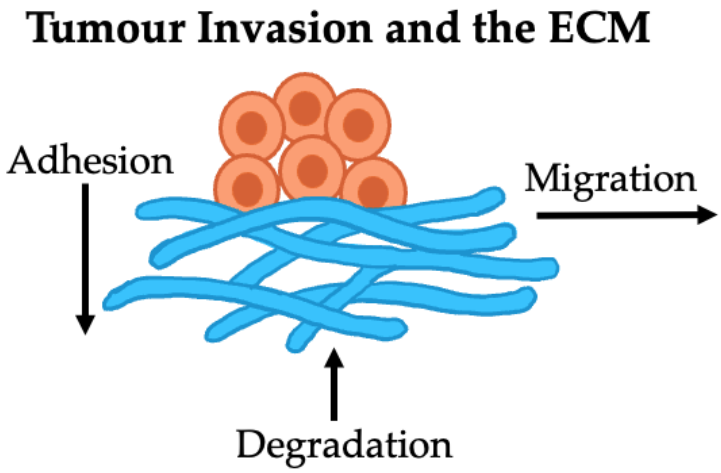

Figure 1.1: Schematic illustration of the key processes in tumour invasion through the ECM. Tumour cells must first adhere to the ECM to gain traction, then degrade the surrounding matrix to open space, and finally migrate forward. This sequence of traction, degradation, and migration drives the invasive advance.

time. The function $D(u, m)$ specifies how tumour motility depends on the local densities of tumour and ECM, while $r(u, m)$ represents local tumour growth and $g(u, m)$ describes ECM dynamics, such as degradation. Many recent models have taken this form, with different choices of the diffusion function: for instance, volume-filling models [18] incorporate crowding by both tumour and ECM, while degenerate cross-diffusion models [19] account for hindrance by ECM alone.

Yet the ECM is not simply a passive barrier during tumour invasion; it also facilitates progression by providing a scaffold for adhesion and migration [3, 4]. Tumour cells require a certain degree of matrix structure in order to move efficiently. This implies that motility is strongest at intermediate ECM levels and suppressed when the ECM is either absent or overly dense—a pattern that lies beyond the scope of linear or monotonic diffusion models.

Moreover, to enhance biological realism, it is important to consider the potential for ECM regeneration following degradation, as observed in biological contexts such as wound healing and tissue remodelling, where structural matrix proteins are rebuilt after damage.

To capture these dynamics, we introduce a new coupled model to describe

tumour invasion through the ECM:

$$\frac{\partial u}{\partial t} = \nabla \cdot (D\, m(1-m)\, \nabla u) + ru(1-u), \tag{1.0.3a}$$

$$\frac{\partial m}{\partial t} = \alpha(1-m) - \lambda u m, \tag{1.0.3b}$$

where $u(x,t)$ denotes the tumour cell density and $m(x,t)$ the ECM density, with $x \in \mathbb{R}^d$ denoting spatial position in multiple dimensions and t time. The nonlinear diffusion term $m(1-m)$ reflects that movement is suppressed when the matrix is either too sparse or too dense, but maximised at intermediate levels. Tumour proliferation is described by logistic growth, while ECM dynamics balance degradation by tumour cells with regeneration toward a homeostatic state.

It should be noted that, due to the novel structure of our model in explaining diffusion and incorporating the possibility of regeneration, there are no established biological values for its parameters. Thus, the analysis we present is carried out for a nondimensional system from this point onward.

The ECM dynamics are governed by the balance of two processes: degradation, arising from direct interactions between tumour cells and the surrounding matrix, and regeneration, reflecting the natural capacity of tissue to recover. The degradation is captured by the term $-\lambda u m$, with $\lambda > 0$ the degradation rate, while regeneration is represented by the term $\alpha(1-m)$, with $\alpha > 0$ the regeneration rate, driving the ECM density towards saturation, that is $m = 1$—corresponding biologically to a healthy, saturated matrix at full density—in the absence of tumour activity.

The aim of this dissertation is to provide a first step toward understanding how ECM dynamics regulate tumour invasion—through resistance to spread, provision of structural support for migration, and the capacity to regenerate and remodel. Specifically, we investigate how variations in the initial ECM density m_0, changes in the rate of degradation, and the presence or absence of regeneration affect the propagation speed of the tumour front. By combining travelling–wave analysis with numerical simulations, this study establishes a foundation for future work on the role of nonlinear diffusion and ECM recovery in tumour progression.

1.1 Objectives and main contributions

In this dissertation, we present a new nonlinear reaction–diffusion PDE model for tumour invasion that explicitly accounts for interactions with the ECM. Due to the novelty of the formulation, and for tractability, we restrict our study to a one–dimensional setting:

in which invasion is described along a single spatial direction.

The model incorporates two key features not present in earlier approaches:

1. **Double cross–degeneracy in diffusion**, ensuring that tumour motility ceases when the ECM is either absent or excessive, thereby enforcing the requirement of an intermediate ECM level for migration.

2. **A regenerative source term for the ECM**, reflecting the natural ability of tissue to repair itself — a mechanism not included in previous models for tumour-ECM modelling.

These features extend existing invasion frameworks and introduce new mathematical challenges. The contributions of this dissertation are threefold:

- **Travelling–wave analysis**: derivation of reduced systems and classification of fixed points under different regeneration regimes.

- **Asymptotic analysis**: investigation of invasion behaviour in parameter limits, highlighting how degeneracy and regeneration affect wave speed.

- **Numerical simulations**: systematic exploration of the dynamics across different initial ECM densities and parameter values, λ and α, validating analytical insights and revealing new qualitative behaviours.

Through this combined analytical–numerical approach, we characterise how nonlinear diffusion and ECM regeneration shape tumour invasion dynamics. This represents the first analysis of this form of model from both analytical and numerical perspectives.

1.2 Prior related work

To motivate the model developed in this work, we review a sequence of mathematical models that have influenced its formulation. We first examine single-

species models, which capture the essential mechanics of invasion in a homogeneous population. We then turn to multi-species models that explicitly represent environmental interactions, such as competition with normal cells or ECM degradation. Each of these models captures important biological or structural features of tumour invasion, and together they illustrate the limitations and insights that have informed the present framework, as well as possible future directions. For consistency, all models are presented in nondimensional form.

1.2.1 Classical and porous reaction–diffusion models

Fisher–Kolmogorov–Petrovskii–Piskunov (FKPP): The FKPP is among the earliest and the most influential reaction–diffusion models for population spread, introduced independently by R. A. Fisher and Kolmogorov, Petrovskii, and Piskunov [17] in 1937. The equation combines random motility, represented by a linear diffusion term, with density-limited proliferation, represented by a logistic growth term:

$$\frac{\partial u}{\partial t} = \frac{\partial^2 u}{\partial x^2} + u(1-u), \tag{1.2.1}$$

where $u(x,t) \in [0,1]$ denotes the cell density. The equation admits travelling–wave solutions, and under the assumption of compact initial conditions one can establish a minimal wave speed $c_{\min} = 2$; in addition, the model possesses a closed-form solution for a very specific wave speed and initial condition [20], although such solutions do not exist in general. Owing to its simplicity, the FKPP model has been widely applied across disciplines, including tumour growth [21], wound healing [22], and ecological phenomena such as rainforest expansion [23]. The model has also been extensively analysed for its stability properties, contributing to its status as a well-studied and widely applied framework [24].

Nevertheless, it has clear limitations: it is restricted to a single species, lacks any environmental feedback, and produces travelling–waves with infinite spatial support, leading to unbounded spread that cannot capture tumours with finite boundaries.

Porous FKPP (pKPP): An extension of the classical FKPP model that introduces a form of spatial guidance for tumour growth is the pKPP model [25]. Here, diffusion is nonlinear and degenerate, allowing tumour cells to preferentially spread into regions where the tumour is already present. This is achieved by taking the

diffusion coefficient to depend on tumour density as $D(u) = u^m$ with $m > 1$, giving

$$\frac{\partial u}{\partial t} = \frac{\partial}{\partial x}\left(u^m \frac{\partial u}{\partial x}\right) + u(1-u). \tag{1.2.2}$$

The diffusivity vanishes as $u \to 0$, producing compactly supported travelling–waves and preventing spread into tumour-free regions.

Similar to the classical FKPP equation, the pKPP equation retains analytical tractability. Phase-plane and matched asymptotic analyses show that the reaction term plays the dominant role in determining the shape of the travelling–wave, while the nonlinear diffusion acts as a correction term, guiding the invasion front into partially invaded regions [25]. The pKPP model shares the same limitations as the classical FKPP in that it is a single-species framework without environmental feedback.

Moving boundary problems for single species: Although not directly relevant to the present work, another way to formulate tumour growth models is through moving-boundary approaches, in which the boundary is treated as a moving interface governed by flux or balance conditions. Variants of the Fisher–KPP and porous Fisher–KPP equations, known as Fisher–Stefan [26] and Porous–Fisher–Stefan [27], have been studied in this setting and show that tumour fronts may expand or recede entirely—a phenomenon termed the *spreading–vanishing dichotomy* [28]. While these models offer insight, they pose analytical challenges and largely reformulate dynamics already captured in our system, which motivates us not to pursue them further.

1.2.2 Environmental effects and the *pH* gradient hypothesis

Gatenby–Gawlinski et al.: The model by Gatenby and Gawlinski [29] was one of the first to explicitly incorporate environmental interactions into tumour invasion modelling, aiming to explain how a tumour could actively degrade and penetrate the surrounding tissue. This pioneering work was based on the *Warburg effect* [30], in which tumour cells acidify the microenvironment through altered metabolism, producing lactic acid that is toxic to surrounding healthy cells. The resulting cell death reduces mechanical resistance and thereby facilitates further tumour spread.

The model is given be the form

$$\frac{\partial n}{\partial t} = \beta n(1-n) + \frac{\partial}{\partial x}\left[\mu(1-h)\frac{\partial n}{\partial x}\right], \tag{1.2.3a}$$

$$\frac{\partial h}{\partial t} = h(1-h-\alpha l), \tag{1.2.3b}$$

$$\frac{\partial l}{\partial t} = \gamma(n-l) + \frac{\partial^2 l}{\partial x^2}, \tag{1.2.3c}$$

where $n(x,t)$ denotes tumour cell density, $h(x,t)$ is the density of healthy cells, and $l(x,t)$ is the lactic acid concentration, with parameters $\beta \geq 0$ for the tumour proliferation rate, $\mu \geq 0$ for the motility coefficient, $\alpha \geq 0$ for the acid–mediated killing rate of healthy cells, and $\gamma \geq 0$ the acid turnover rate.

Numerical simulations revealed a distinctive *interstitial gap*—a region devoid of healthy cells that forms ahead of the invading tumour front—in agreement with experimental observations. This model laid important groundwork for subsequent environmental feedback frameworks, although it assumed that tumour cells were unaffected by acidity, an oversimplification that neglects evidence that tumours can also be harmed by extreme pH levels. Moreover, the three–species interaction terms could be simplified without losing the essential acid–mediated invasion mechanism [19].

Colson et al.: Colson et al. [19] simplified the Gatenby–Gawlinski framework by removing the acid field and replacing the healthy-cell variable with an ECM field, yielding a two–equation model presented primarily as a reduction of the original three–species system rather than a new mechanistic justification. In nondimensional form,

$$\frac{\partial n}{\partial t} = \frac{\partial}{\partial x}\left[(1-m)\frac{\partial n}{\partial x}\right] + (1-n)n, \tag{1.2.4a}$$

$$\frac{\partial m}{\partial t} = -\kappa m n, \tag{1.2.4b}$$

where $n(x,t)$ is the tumour density, $m(x,t)$ the ECM density, and $\kappa > 0$ the ECM degradation rate; the effective diffusivity of tumour cells degenerates as $m \to 1$, limiting invasion into ECM-saturated regions. Despite the degenerate cross–diffusion, an analytical expression for the invasion speed is available only when the initial ECM density satisfies $0 < m_0 < 1$, corresponding biologically to an existing but partially degraded ECM. At the same time, the model leaves

important biology unresolved because tumour motility depends on ECM availability yet the predicted speed is independent of the rate of degradation, which is a factor that influences the density of the ECM over time.

Browning et al. A model closely related to that of Colson et al. was developed by Browning et al. [31], in which tumour cell proliferation was also made dependent on the availability of the ECM. The model is written as

$$\frac{\partial u}{\partial t} = \frac{\partial}{\partial x}\left[(1-m)\frac{\partial u}{\partial x}\right] + u(1-u-m), \tag{1.2.5a}$$

$$\frac{\partial m}{\partial t} = -\gamma u m, \tag{1.2.5b}$$

where $u(x,t)$ denotes tumour cell density, $m(x,t)$ is the ECM density and γ is the rate degradation. A key addition in this model is the proliferation term $u(1-u-m)$, which is limited by both tumour crowding and ECM density, a mechanism often referred to as *volume filling* [32].

An analysis of this model by El-Hachem et al. [18] derived asymptotic limits for the invasion speed and demonstrated its dependence on the ECM degradation rate (see Table C.1. Although not incorporated directly into the present framework, these results motivate our examination of asymptotic behaviour to understand how degradation influences invasion dynamics.

Crossley et al. (Coarse-grained model of cell invasion). The coarse-grained model of tumour invasion proposed by Crossley et al. [33] introduced a mechanism distinct from the pKPP framework by adding an advective flux term that drives movement down the gradient of the ECM. In nondimensional form, the system can be written as

$$\frac{\partial u}{\partial t} = \frac{\partial}{\partial x}\left[(1-m)\frac{\partial u}{\partial x} + u\frac{\partial m}{\partial x}\right] + u(1-u-m), \tag{1.2.6a}$$

$$\frac{\partial m}{\partial t} = -\lambda m u, \tag{1.2.6b}$$

where $u(x,t)$ denotes tumour density, $m(x,t)$ the ECM density, and $\lambda > 0$ the ECM degradation rate. The first term in the flux represents ECM-dependent diffusion of tumour cells, while the second represents advection down the ECM gradient. Asymptotic and numerical analysis showed that, for very small or very

Model	$D(u,m)$	$r(u,m)$
FKPP	$\partial_{xx}u$	$u(1-u)$
pKPP (pKPP)	$\partial_x\left(u^m u_x\right)$	$u(1-u)$
Colson [19]	$\partial_x\left((1-m)\,u_x\right)$	$u(1-u)$
Browning [31, 18]	$\partial_x\left((1-m)\,u_x\right)$	$u(1-u-m)$
Equations ((??)) and ((??))	$\partial_x\left(\,m(1-m)\,u_x\right)$	$u(1-u)$

Table 1.1: Description of the diffusion and proliferation terms considered by models in the prior work reviewed in this study.

large degradation, the invasion dynamics reduce to those of simpler models such as FKPP, Colson et al. [19], or Browning et al [31]. Thus, while advective dispersal can introduce new effects, its qualitative behaviour is captured more simply by these models, and we do not pursue it further here. A summary of the diffusion and proliferation terms across the reviewed models is provided in Table 1.1, highlighting the structural differences that motivate our formulation.

Chapter 2

Model formulation

In this chapter, we introduce the non-dimensional mathematical model that forms the foundation of our study. The aim is to develop a biologically motivated framework that captures key features of tumour invasion into the surrounding ECM. In particular, we account for the ECM's dual role in tumour invasion: it provides the substrate required for tumour cell migration, but must also be degraded for invasion to progress. We further incorporate the ability of the ECM to regenerate, reflecting the body's natural capacity to repair and remodel damaged tissue. The derivation of the non-dimensional system from its dimensional counterpart is presented in Appendix A.1. Throughout this dissertation, however, we focus exclusively on the non-dimensional model in one spatial direction, which provides the basis for the analytical and numerical investigations that follow.

2.1 Mathematical model

To model interactions of the tumour with the ECM that are both spatially and dynamically coupled in continuum, we consider a system of the form:

$$\frac{\partial u}{\partial t} = \frac{\partial}{\partial x}\left(\underbrace{D(u,m)}_{\substack{\text{diffusion}\\ \text{coefficient}}}\frac{\partial u}{\partial x}\right) + \underbrace{r(u,m)}_{\substack{\text{tumour}\\ \text{proliferation}}}, \tag{2.1.1}$$

$$\frac{\partial m}{\partial t} = \underbrace{f(u,m)}_{\substack{\text{ECM}\\ \text{recovery}}} - \underbrace{h(u,m)}_{\substack{\text{ECM}\\ \text{degradation}}}. \tag{2.1.2}$$

Here, $u(x,t)$ denotes the tumour cell density and $m(x,t)$ the ECM density

at position x and time t. The functions appearing in the system are defined on biologically meaningful domains and satisfy natural positivity conditions:

- $D(u,m) \geq 0$: effective diffusion coefficient regulating tumour motility,
- $r(u,m) \geq 0$: tumour proliferation, vanishing when $u = 0$,
- $f(u,m) \geq 0$: ECM recovery aided by healthy tissue, strongest when $m \ll 1$ and tending to zero as $m \to 1$,
- $h(u,m) \geq 0$: ECM degradation, vanishing when $u = 0$ or $m = 0$.

This coupled structure allows us to capture both the mechanical and biological feedback between tumour progression and the ECM microenvironment. For simplicity, explicit tumour cell death is not included in this formulation, though it represents a natural extension for future work.

Tumour cell proliferation

To model tumour expansion, we introduce a source term that captures tumour cell proliferation. For this purpose, we adopt a logistic growth law, which reflects the fact that proliferation requires an initial population of abnormal cell [34, 35] and saturates at high densities due to crowding [36] or resource limitation [37]. Proliferation is assumed to be independent of ECM density, since the ECM regulates motility rather than growth, and does not compete directly with tumour cells for proliferation. Specifically,

$$r(u,m) = u\,(1-u). \tag{2.1.3}$$

Compared with alternatives such as linear [38] or Allee-type kinetics [39, 40], the logistic form is preferable: linear growth lacks saturation, while Allee dynamics impose a critical threshold for persistence. The logistic law instead provides a minimal, biologically grounded description of bounded proliferation and is consistent with established approaches in tumour invasion modelling [17, 19, 25, 26].

ECM-dependent diffusion

A central feature of our model is the incorporation of ECM-regulated tumour motility through a nonlinear diffusion term. Experimental studies have shown

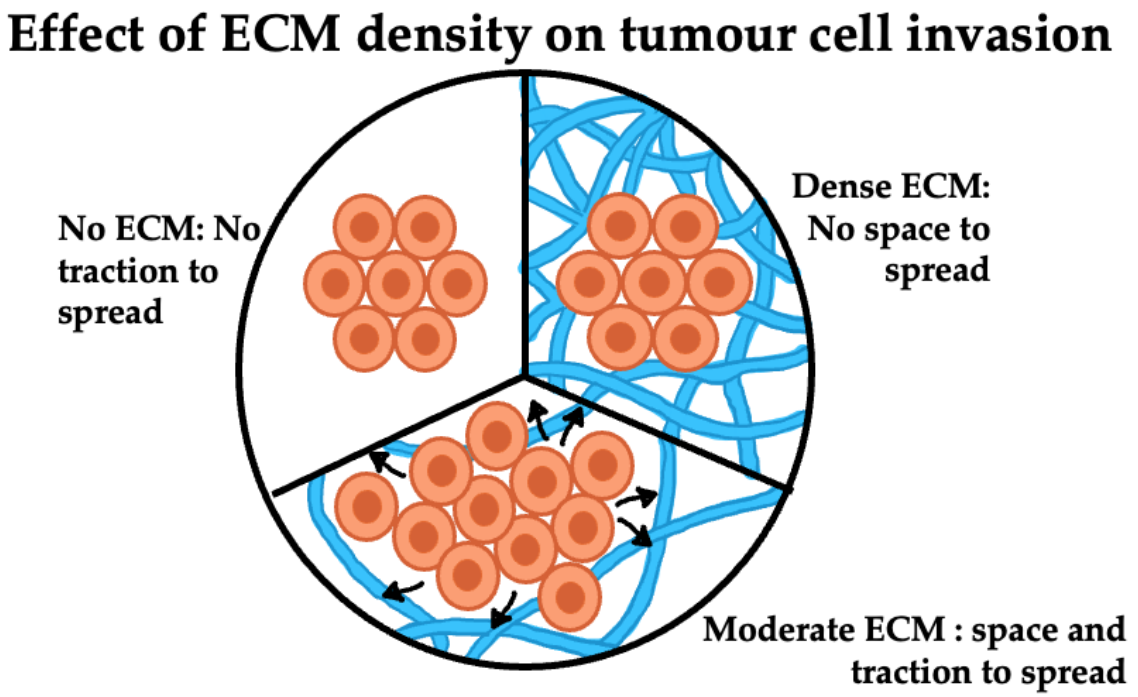

Figure 2.1: Effect of ECM density on tumour cell invasion. Schematic illustration showing that tumour cells cannot spread in the absence of ECM (no traction) or in overly dense ECM (no space), while moderate ECM provides both traction and space for migration.

that tumour cells require the ECM to generate traction for migration, yet encounter strong resistance when the ECM is overly compact [3, 4]. As illustrated in Figure 2.1, cells are effectively immobilised both in the absence of ECM, where they cannot adhere, and in regions of high density, where fibres act as a physical barrier. In contrast, invasion is favoured when the ECM is present at moderate levels, providing both anchorage and space for movement.

To represent this biphasic effect, we adopt the diffusion law

$$D(u, m) = m\,(1 - m), \tag{2.1.4}$$

which vanishes when the ECM is depleted ($m = 0$) or saturated ($m = 1$), and attains its maximum at $m = 0.5$, corresponding to the regime of optimal invasion. Although this structure introduces degeneracy at the boundaries, it provides a natural representation of how the ECM can both facilitate and hinder tumour spread depending on its density.

ECM degradation

ECM breakdown is driven by tumour–ECM interactions, where cancer cells degrade the surrounding structure to facilitate invasion. Biologically, this can occur in two principal ways: indirectly, via the secretion of enzymes or acidic by-products that diffuse into and dissolve the ECM [41], or directly, through contact-mediated degradation at the tumour–ECM interface [42]. Following the simplification introduced by Colson et al. [19], we focus on the latter and model degradation as a local effect of direct tumour–ECM contact. This avoids introducing additional diffusive variables, such as enzyme or acid concentrations, while still capturing a key mode of breakdown.

Accordingly, we adopt the form

$$h(u, m) = \lambda\, u\, m, \tag{2.1.5}$$

where $\lambda > 0$ is the ECM degradation rate. This captures the requirement that degradation only occurs when both tumour cells and ECM are simultaneously present.

ECM recovery

To complete the model, we introduce a source term governing regeneration of the ECM. Biologically, the ECM has the capacity to repair itself following degra-

dation, a process observed in contexts such as wound healing [22] and tissue remodelling [43]. The precise mechanism and its influence on tumour progression remain uncertain, so for simplicity we assume that regeneration is supplied externally by surrounding healthy tissue rather than by intrinsic ECM proliferation. We represent this process by a density-dependent term of the form

$$f(u, m) = \alpha (1 - m), \tag{2.1.6}$$

where $\alpha \geq 0$ is the regeneration rate. This formulation ensures that recovery is strongest when the ECM is depleted and diminishes as $m \to 1$. It also prevents unbounded accumulation in the long run, since regeneration naturally slows once the ECM approaches full density and is suppressed if the ECM becomes overly saturated. This functional form therefore captures a biologically realistic balance between recovery and limitation.
Within this framework, we consider two cases:

With regeneration $\alpha > 0$: In this regime, the ECM continually attempts to restore its structure, modifying the environment left behind the advancing tumour front. As we shall see in the following section, the inclusion of regeneration alters the travelling-wave dynamics, limiting explicit analysis and necessitating numerical investigation.

No regeneration $\alpha = 0$: When regeneration is absent, ECM degraded by the tumour cannot be restored. The resulting ECM profile is determined solely by the advancing front, which leaves behind a permanently depleted region. Although this case is biologically less realistic, it provides a useful benchmark, as it isolates the role of ECM degradation and permits explicit results to be obtained for the minimal travelling-wave speed of the tumour. This treatment of ECM dynamics is consistent with that adopted in previous models [19, 31, 33].

We do not assume ECM recovery to be constant, that is $f(u, m) = K > 0$, since such a formulation would imply regeneration at a fixed rate independent of ECM density, leading to unbounded growth of the ECM, which is not biologically realistic. This case is briefly discussed in Appendix C.1 but does not form part of the main analysis.

2.2 Initial and boundary conditions

To complete the modelling framework, we specify both the initial conditions for tumour and ECM densities and the boundary conditions, which are biologically motivated on a finite section of tissue represented by the domain $[0, L]$.

With the knowledge that tumour invasion begins from a cluster of abnormal cells [34, 35], we require an initial condition that represents a finite population which gradually extends into the surrounding ECM. Popular alternatives such as a step function or an exponential profile are unsuited to this purpose: the step function, though mathematically simple, fails to capture the gradual transition from tumour-present to tumour-free regions, while the exponential profile is smooth but extends indefinitely into the ECM, contradicting the assumption of a confined initial cluster.

For this reason, we adopt a hyperbolic tangent form,

$$u(x,0) = u_0 \cdot \tfrac{1}{2}\big[1 - \tanh(x - pL)\big], \tag{2.2.1}$$

where u_0 sets the initial size of the cluster and the shift parameter pL, with $0 < p < 1$, positions the cluster within the domain. The factor $1/2$ yields a normalised profile for the growth, ensuring that the transition is scaled smoothly between tumour-present and tumour-free regions. We set $p = 0.4$, ensuring that the initial cluster is positioned sufficiently within the domain so that tumour cells have already established locally while still leaving adequate space for invasion to develop. While our choice of initial condition does not preclude a cluster from evolving near the boundary—as $u(L,0) > 0$—the profile decays more rapidly than an exponential owing to its semi-compact character. This means that, even though the tail is nonzero, cells are effectively forced to disappear much more quickly than under an exponential profile. Nevertheless, for reasons of biological realism, we avoid analysing cases in which the cluster is initiated too close to the boundary.

For the ECM, we assume a spatially uniform initial distribution,

$$m(x,0) = m_0, \qquad m_0 \geq 0, \tag{2.2.2}$$

representing a homogeneous tissue environment prior to invasion. Here $m_0 = 0$ corresponds to a completely degraded ECM, while $m_0 = 1$ represents a fully intact environment.

Consistent with this framework, we impose no-flux boundary conditions at the edges of the region under consideration, reflecting the assumption that the tissue section is isolated from its surroundings so that no tumour cells enter or leave through the boundaries. Because tumour motility depends on the local ECM density, the condition must be imposed on the full flux term rather than on the spatial derivative alone. Specifically, we enforce

$$m(1-m)\frac{\partial u}{\partial x} = 0 \quad \text{at } x = 0, L, \tag{2.2.3}$$

which ensures that tumour cells do not pass through the domain edges.

Since our model does not incorporate diffusion for the ECM, its evolution is governed solely temporally by local regeneration and degradation. We therefore do not impose any boundary condition for $m(x,t)$.

Chapter 3

Travelling wave analysis

In this chapter, we adopt a travelling wave formulation for our model to study tumour invasion and its interaction with the surrounding ECM. Instead of analysing the full time-dependent PDE system, we reformulate the problem in a moving coordinate frame that follows the invasion front. This approach is well suited to long-term invasion dynamics, as it represents the tumour as a fixed profile advancing into healthy tissue at constant speed. Compared with moving boundary methods [26, 27]—which capture similar dynamics but often introduce analytical and numerical complications—the travelling wave formulation is simpler. It reduces the PDE system to a set of ordinary differential equations (ODEs), preserving the essential features of invasion while allowing the use of fixed-point (FP) classification and stability analysis, which we develop in the following sections.

3.1 Travelling wave formulation

To describe tumour invasion as a travelling wave, we introduce the moving coordinate

$$\xi = x - ct, \qquad c > 0,$$

where c denotes the constant speed of propagation of the tumour front from left to right. We then assume that the tumour and ECM densities depend only on ξ, writing

$$u(x,t) = U(\xi), \qquad m(x,t) = M(\xi).$$

Under this transformation the derivatives become

$$\frac{\partial}{\partial t} = -c\,\frac{d}{d\xi}, \qquad \frac{\partial}{\partial x} = \frac{d}{d\xi},$$

which reduces the PDE system to the coupled ODEs

$$\frac{d}{d\xi}\left(M(1-M)\,\frac{dU}{d\xi}\right) + c\,\frac{dU}{d\xi} + U(1-U) = 0, \tag{3.1.1a}$$

$$c\,\frac{dM}{d\xi} + \lambda UM - \alpha(1-M) = 0. \tag{3.1.1b}$$

To impose asymptotic boundary conditions, we require the travelling wave profiles $(U(\xi), M(\xi))$ to connect biologically relevant steady states ahead of and behind the wave.

For the tumour density, the profile must connect the invaded region behind the front, where the tumour saturates at its scaled carrying capacity, to the uninvaded region ahead, where the tumour is absent. Accordingly, we impose

$$\lim_{\xi\to-\infty} U(\xi) = 1, \tag{3.1.2a}$$

$$\lim_{\xi\to+\infty} U(\xi) = 0. \tag{3.1.2b}$$

For the ECM, the asymptotic boundary conditions must connect its state before and after tumour invasion. These are determined by the states of the ECM dynamics at the two ends of the wave:

$$\frac{dM}{d\xi} = \begin{cases} \alpha(1-M) - \lambda M, & \text{behind the tumour front } (U \approx 1), \\ \alpha(1-M), & \text{ahead of the tumour front } (U = 0). \end{cases} \tag{3.1.3}$$

From these dynamics, the asymptotic boundary conditions follow, depending on whether regeneration is present.

No regeneration ($\alpha = 0$):

$$\lim_{\xi\to-\infty} M(\xi) = 0, \tag{3.1.4a}$$

$$\lim_{\xi\to+\infty} M(\xi) = m_0, \quad m_0 \in [0,1]. \tag{3.1.4b}$$

Here the ECM is eventually fully degraded behind the tumour front, irrespective of m_0 or λ. Ahead of the front, the ECM remains fixed at its initial level, with the restriction $m_0 \leq 1$ arising from the nondimensionalisation that sets unity as the maximal attainable density.

With regeneration ($\alpha > 0$):

$$\lim_{\xi \to -\infty} M(\xi) = \frac{\alpha}{\alpha + \lambda}, \tag{3.1.5a}$$

$$\lim_{\xi \to +\infty} M(\xi) = 1. \tag{3.1.5b}$$

In this case, regeneration counteracts degradation behind the tumour front, driving the ECM to the stable steady state $M = \alpha/(\alpha + \lambda)$, so that a positive ECM level persists even after invasion. Ahead of the front, recovery restores the ECM to full saturation regardless of its initial level, consistent with the ability of healthy tissue to repair itself.

Together, these asymptotic boundary conditions define a travelling invasion front in which the tumour profile connects invaded to uninvaded tissue, while the ECM profile reflects either complete degradation or partial recovery depending on whether regeneration is absent or present.

3.2 Desingularisation and ODE reformulation

The travelling wave equations (3.1.1a)–(3.1.1b) are singular at $M = 0$ and $M = 1$, corresponding to fully degraded and fully intact ECM, respectively. At these points the effective diffusion coefficient $M(1 - M)$ vanishes, causing the diffusion operator to degenerate and rendering the system unsuitable for direct analysis.

To overcome this difficulty, we apply a standard desingularisation procedure, following related invasion models [18, 19, 33]. We introduce the independent desingularising map $y = \phi(\xi)$, defined by

$$\frac{dy}{d\xi} = \frac{1}{M(\xi)(1 - M(\xi))}. \tag{3.2.1}$$

We then define the dependent variables

$$\tilde{U}(y) = U(\phi^{-1}(y)), \qquad \tilde{M}(y) = M(\phi^{-1}(y)), \tag{3.2.2}$$

and, by applying the chain rule, the travelling wave equations transform into

$$\frac{d^2\tilde{U}}{dy^2} + c\,\frac{d\tilde{U}}{dy} + \tilde{U}(1 - \tilde{U})\tilde{M}(1 - \tilde{M}) = 0, \tag{3.2.3a}$$

$$\frac{d\tilde{M}}{dy} - \tfrac{1}{c}\,\tilde{M}(1 - \tilde{M})\big(\lambda\tilde{U}\tilde{M} - \alpha(1 - \tilde{M})\big) = 0. \tag{3.2.3b}$$

where the degeneracies at $M = 0$ and $M = 1$ have now been removed.
The asymptotic boundary conditions, inherited from the travelling wave formulation, are

$$\lim_{y\to-\infty} \tilde{U}(y) = 1, \tag{3.2.4a}$$

$$\lim_{y\to+\infty} \tilde{U}(y) = 0. \tag{3.2.4b}$$

Similarly, for the ECM, the boundary conditions depend on the presence of regeneration:

- **No regeneration ($\alpha = 0$):**

$$\lim_{y\to-\infty} \tilde{M}(y) = 0, \tag{3.2.5a}$$

$$\lim_{y\to+\infty} \tilde{M}(y) = m_0, \quad m_0 \in [0,1]. \tag{3.2.5b}$$

- **With regeneration ($\alpha > 0$):**

$$\lim_{y\to-\infty} \tilde{M}(y) = \frac{\alpha}{\alpha+\lambda}, \tag{3.2.6a}$$

$$\lim_{y\to+\infty} \tilde{M}(y) = 1. \tag{3.2.6b}$$

Finally, introducing the auxiliary variable $\tilde{P}(y) = d\tilde{U}/dy$ and dropping asterisks, for notational simplicity, we obtain the desingularised first-order system:

$$U' = P, \tag{3.2.7a}$$

$$P' = -cP - U(1-U)M(1-M), \tag{3.2.7b}$$

$$M' = \tfrac{1}{c}\, M(1-M)(\lambda UM - \alpha(1-M)), \tag{3.2.7c}$$

where (U, P, M) depends on y and primes denote derivatives with respect to this variable.
We will henceforth use this desingularised system (3.2.7) as the basis for the FP and stability analysis carried out in this chapter.

3.3 Fixed point analysis

We begin by analysing the FP of the desingularised system (3.2.7), restricting attention to those that are also spatio–temporal equilibria of the original nondimensional PDE system (**??**). These represent biologically relevant states that provide

a meaningful interpretation of tumour invasion dynamics, such as fully invaded tumour regions and tumour-free tissue with varying ECM density.

To characterise the local behaviour near these FP, we perform a linear stability analysis. Using the state vector (U, P, M), the Jacobian of the desingularised system (3.2.7) is defined by

$$J = \frac{\partial(U', P', M')}{\partial(U, P, M)}.$$

Evaluating this gives

$$J = \begin{pmatrix} 0 & 1 & 0 \\ a_1 & -c & a_2 \\ b_1 & 0 & b_2 \end{pmatrix}, \tag{3.3.1}$$

where

$$a_1 = -(1-2U)\,M(1-M), \qquad a_2 = -(1-U)\,U\,(1-2M),$$
$$b_1 = \lambda\, M^2(1-M), \qquad b_2 = -(3\lambda U + 3\alpha)M^2 + (2\lambda U + 4\alpha)M - \alpha.$$

The eigenvalues of J determine the stability type of each FP. In what follows, we analyse them separately for two cases: the absence of regeneration ($\alpha = 0$) and the presence of regeneration ($\alpha > 0$).

3.3.1 No regeneration $(\alpha = 0)$

In the absence of ECM regeneration, the desingularised system (3.2.7) admits two biologically relevant classes of FPs:

$$(U, P, M) = (1, 0, 0), \qquad (U, P, M) = (0, 0, \bar{M}), \quad \bar{M} \in (0, 1). \tag{3.3.2}$$

FP $(1, 0, 0)$: Saturated tumour with no ECM present. The Jacobian (A.0.15) evaluated at this point has eigenvalues

$$\{0, 0, -c\}, \tag{3.3.3}$$

indicating a non-hyperbolic equilibrium with a single stable direction. The pair of zero eigenvalues reflects degeneracy in the (U, M) plane, and hence the local behaviour cannot be fully characterised using linearisation alone.

FP $(0, 0, \bar{M})$: Tumour-free tissue with ECM density $\bar{M} \in (0, 1)$. This is not an isolated equilibrium but rather a continuum, forming a one-dimensional line of

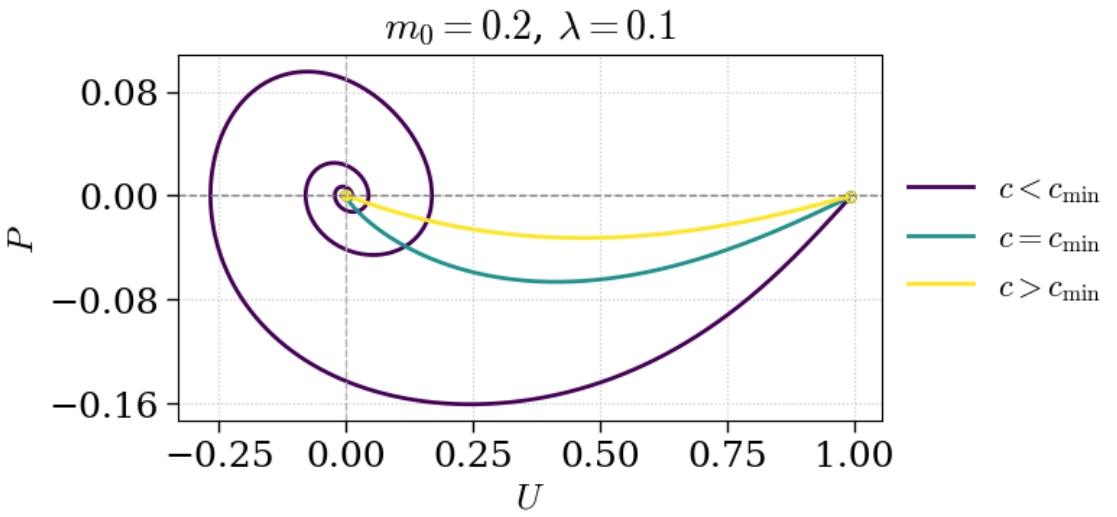

Figure 3.1: Phase–space projection of the desingularised system (3.2.7) onto the (U, P)–plane for $m_0 = 0.2$ and $\lambda = 0.1$. The trajectories illustrate the transition from a stable configuration to either a stable node or a stable spiral as the travelling wave speed c exceeds the minimal value $c_{\min} = 2\sqrt{\bar{M}(1-\bar{M})}$. Further details of the numerical methods and parameter choices are provided in Chapter 5 and Appendix B.3.

equilibria parameterised by $\bar{M}$. The corresponding eigenvalues at each point along this line are

$$\mu_1 = 0, \qquad \mu_{2,3} = \frac{-c \pm \sqrt{c^2 - 4\bar{M}(1-\bar{M})}}{2}. \tag{3.3.4}$$

This FP is always linearly stable, since the real parts of the eigenvalues are non-positive. However, its qualitative stability depends on the ECM density. When

$$c^2 > 4\bar{M}(1-\bar{M}), \tag{3.3.5}$$

the equilibrium is a stable node, whereas if

$$c^2 < 4\bar{M}(1-\bar{M}), \tag{3.3.6}$$

it becomes a stable spiral. Both behaviours were confirmed in our phase–space projections (Figure 3.1), where trajectories approaching the equilibrium manifested either as nodes or as spirals depending on the parameter regime. Although both classes of FPs are stable yet non-hyperbolic, a rigorous characterisation of

connecting trajectories would require invariant manifold theory, which lies beyond the scope of this study. Nevertheless, the phase–space projections reveal biologically feasible trajectories confined to the region

$$U \geq 0, \qquad M \geq 0, \qquad P \leq 0, \tag{3.3.7}$$

which connect tumour-free and tumour-saturated states. This provides evidence for the existence of a minimal invasion speed,

$$c_{\min} = 2\sqrt{\bar{M}(1-\bar{M})}, \tag{3.3.8}$$

below which travelling wave solutions cannot be sustained. This indicates that the rate of tumour progression is determined solely by the ECM state, represented by the equilibrium density $\bar{M}$, in line with related invasion models [19, 31].

3.3.2 Regeneration source$(\alpha > 0)$

In the presence of regeneration, the desingularised system (3.2.7) admits two biologically relevant classes of FPs:

$$(U,P,M) = (0,0,1), \qquad (U,P,M) = (1,0,M^*), \quad M^* = \frac{\alpha}{\alpha+\lambda}. \tag{3.3.9}$$

FP $(0,0,1)$: Tumour-free tissue with fully intact ECM. At this point, the Jacobian (A.0.15) has eigenvalues

$$\{0,0,-c\}, \tag{3.3.10}$$

yielding a non-hyperbolic equilibrium with one stable direction. This behaviour mirrors the tumour-free equilibrium encountered in the no-regeneration case.
FP $(1,0,M^*)$: Saturated tumour with partially degraded ECM. The eigenvalues at this point are

$$\mu_1 = b_2, \qquad \mu_{2,3} = \frac{-c \pm \sqrt{c^2 + 4M^*(1-M^*)}}{2}, \tag{3.3.11}$$

with

$$b_2 = -(3\lambda+3\alpha)(M^*)^2 + (2\lambda+4\alpha)M^* - \alpha. \tag{3.3.12}$$

In contrast to the no-regeneration case, this FP is an unstable saddle, as the condition

$$c^2 + 4M^*(1-M^*) > c^2 \tag{3.3.13}$$

ensures the presence of a positive eigenvalue.

Although linear analysis does not provide a closed-form expression for the minimal invasion speed, numerical simulations of the PDE identify a wave speed which, when imposed in the desingularised system, generates connecting trajectories between tumour-free and tumour-saturated states (Figure 3.2). For speeds below this value, the dynamics exhibit spiral approaches to the FP $(1, 0, M^*)$, similar to the behaviour observed in the no-regeneration case, suggesting the existence of a minimal invasion speed even though no closed-form expression could be obtained.

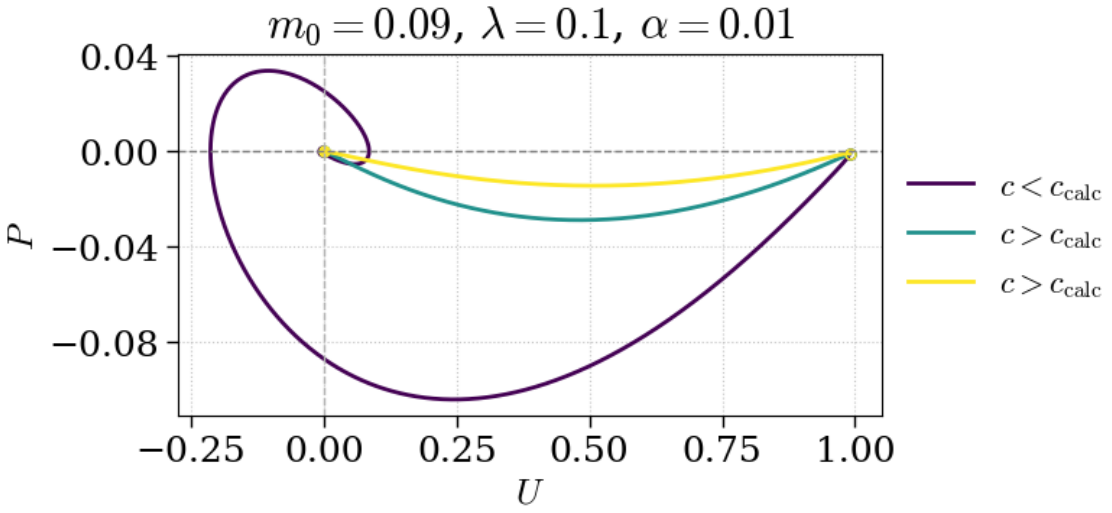

Figure 3.2: Phase–space projection of the system (3.2.7) onto the (U, P)–plane for $m_0 = 0.09$, $\lambda = 0.1$, and $\alpha = 0.01$. The trajectories connect the unstable saturated–tumour FP $(1, 0, M^*)$ to the stable tumour–free state. Since the minimal wave speed cannot be obtained analytically, we use c_{calc}, computed numerically from PDE system (**??**) with initial conditions (2.2.1) and (2.2.2). Further details of the numerical methods and parameter choices are provided in Chapter 5 and Appendix B.3.

Chapter 4

Asymptotic analysis

In this chapter, we investigate the tumour–ECM system in limiting parameter regimes, where the regeneration rate α or the degradation rate λ is taken to be either very large or very small. Such asymptotic analysis isolates the dominant mechanisms of invasion and yields reduced equations that provide insight into the effect of extreme parameter values. Comparable approaches have been employed in related invasion models [18, 33], where such limits yield simplified dynamics and transparent scaling laws with clear biological interpretation.

We begin with the case of no regeneration ($\alpha = 0$), before extending the analysis to the general case with regeneration ($\alpha > 0$).

4.1 No regeneration source ($\alpha = 0$)

To begin our analysis, we use the travelling-wave system derived in the previous section:

$$\frac{d}{d\xi}\left(M(1-M)\frac{dU}{d\xi}\right) + c\frac{dU}{d\xi} + U(1-U) = 0, \tag{4.1.1a}$$

$$c\frac{dM}{d\xi} + \lambda UM = 0, \tag{4.1.1b}$$

with boundary conditions

$$\lim_{\xi\to-\infty} U(\xi) = 1, \tag{4.1.2a}$$

$$\lim_{\xi\to+\infty} U(\xi) = 0, \tag{4.1.2b}$$

$$\lim_{\xi\to-\infty} M(\xi) = 0, \tag{4.1.2c}$$

$$\lim_{\xi\to+\infty} M(\xi) = m_0, \quad m_0 \in [0,1]. \tag{4.1.2d}$$

From the ECM equation (4.1.1b), we apply the variable–separable method to obtain

$$\frac{dM}{M} = -\tfrac{\lambda}{c} U(\xi)\, d\xi. \tag{4.1.3}$$

Integrating this expression from ξ to $+\infty$, and using the far-field boundary condition (4.1.2d), yields the semi–explicit representation

$$M(\xi) \approx m_0 \exp\left(-\tfrac{\lambda}{c}\int_{\xi}^{\infty} U(s)\, ds\right). \tag{4.1.4}$$

This representation expresses the ECM density in terms of the tumour profile U. Biologically, it shows that the ECM at a given position is depleted in proportion to the cumulative tumour density ahead of that point — the larger the integral of U over the downstream region, the greater the local ECM loss.

To proceed analytically, we assume that the tumour density decays exponentially in the far field. That is, we adopt the ansatz

$$U(\xi) \sim e^{-\beta\xi}, \qquad \beta > 0, \tag{4.1.5}$$

which is consistent with the expected behaviour of travelling-wave solutions near the leading edge [44]. Substituting the ansatz (4.1.5) into the semi-explicit representation (4.1.4) and evaluating the integral gives the closed form approximation

$$M(\xi) \approx m_0 \exp\left(-\tfrac{\lambda}{c\beta}\, e^{-\beta\xi}\right). \tag{4.1.6}$$

4.1.1 Weak degradation: $\lambda \to 0^+$

Travelling–wave solutions typically consist of two distinct regions: the front of the wave, where rapid changes occur, and the region behind the wave, where the profile is relatively flat and approaches a constant state.

Considering the front of the wave first, from the closed form (4.1.6) we observe that as $\lambda \to 0^+$,

$$M(\xi) \to m_0. \tag{4.1.7}$$

Substituting this into the tumour equation (4.1.1a) gives

$$m_0(1-m_0)\frac{d^2U}{d\xi^2} + c\frac{dU}{d\xi} + U(1-U) = 0. \tag{4.1.8}$$

which is precisely the FKPP equation in travelling-wave form, with effective coefficients

$$D = m_0(1-m_0), \tag{4.1.9}$$

$$r = 1. \tag{4.1.10}$$

Although this reduction may appear surprising at first, it is consistent with the findings of Crossley et al. [33] in the same limit. It shows that when ECM degradation is very slow, the coupled two-species system for tumour and ECM effectively reduces to a single-species FKPP model describing the tumour alone.

Behind the wave, where the solution is relatively constant, the derivative terms in the dynamics for the tumour (4.1.1a) vanish and the equation reduces to

$$U(1-U) = 0, \tag{4.1.11}$$

and applying the boundary condition (4.1.2a) yields

$$U = 1. \tag{4.1.12}$$

With this, the ECM dynamics simplify to

$$\frac{dM}{d\xi} = -\tfrac{1}{c}M. \tag{4.1.13}$$

This integrates to

$$M(\xi) = m_0 \exp\left(-\tfrac{\lambda}{c}\xi\right), \tag{4.1.14}$$

where the integration constant has been determined by the matching condition at the front, $M(\xi = 0) = m_0$. It should be noted that because the proliferation term in our model does not depend explicitly on ECM, the matched–asymptotic constructions employed by El-Hachem et al. [18] and Crossley et al. [33] cannot be applied to obtain a continuous composite solution. Consequently, the connection between the two regions must be resolved numerically, at least until alternative analytical approaches are developed.

4.1.2 Strong degradation: $\lambda \to \infty$

We now consider the opposite asymptotic regime, corresponding to very rapid ECM degradation. From the semi–explicit form of equation (4.1.1b) we see that as $\lambda \to \infty$, $M(\xi) \to 0$. Substituting this into the tumour equation (4.1.1a), the diffusion term $M(1-M)$ degenerates to zero and, with U also exponentially decaying, the system reduces to the much simpler logistic form

$$c\,\frac{dU}{d\xi} + U(1-U) = 0. \tag{4.1.15}$$

This equation can be solved explicitly as

$$U(\xi) = \frac{1}{1 + Ae^{\xi/c}}, \tag{4.1.16}$$

where A is a constant of integration. Since we are concerned with the behaviour at the front of the wave as $\xi \to +\infty$, the solution reduces asymptotically to

$$U(\xi) \;\sim\; \frac{1}{A}\,e^{-\xi/c}. \tag{4.1.17}$$

To match the expected exponential tail and fix the horizontal shift of the profile, we may set $A = 1$, so that

$$U(\xi) \;\sim\; e^{-\xi/c}, \qquad \xi \to +\infty. \tag{4.1.18}$$

This shows that the solution has the correct exponential decay with rate $\beta = 1/c$, consistent with the anticipated asymptotics, provided $c > 0$.

We now turn to the behaviour behind the front. Introducing the rescaled coordinate $\zeta = \lambda\xi$ to capture the rapid variation of the ECM, the tumour equation reduces in the limit $\lambda \to \infty$ to

$$U(1-U) = 0,$$

so in the invaded region we obtain $U \approx 1$, consistent with the boundary condition at $\xi \to -\infty$. The ECM equation has the same structure as in the weak–degradation case, leading to an exponentially decaying profile behind the front.

In this regime the simulations, see Figure B.2, show a rapid and essentially perfect match to the logistic profile, even for moderate values of λ. This confirms that once degradation is fast enough, the ECM is effectively destroyed throughout the invaded region, leaving no structural support or spatial barrier. With the ECM absent, the tumour population has no medium to interact with and instead competes only with itself, spreading purely according to logistic growth.

4.2 Regeneration source ($\alpha > 0$)

We now extend the asymptotic analysis to incorporate ECM regeneration. The travelling–wave system is

$$\frac{d}{d\xi}\left(M(1-M)\frac{dU}{d\xi}\right) + c\frac{dU}{d\xi} + U(1-U) = 0, \tag{4.2.1a}$$

$$c\frac{dM}{d\xi} + \lambda UM - \alpha(1-M) = 0. \tag{4.2.1b}$$

together with the same boundary conditions as in the no–source case.
The dynamics now depend on two parameters, λ and α. To simplify the analysis, we introduce their ratio

$$\sigma = \frac{\lambda}{\alpha}, \tag{4.2.2}$$

so that the ECM equation becomes

$$\frac{dM}{d\xi} - \frac{\alpha}{c}\left(1 + \sigma U(\xi)\right) M = -\frac{\alpha}{c}. \tag{4.2.3}$$

We again assume exponential decay of the tumour density near the leading edge,

$$U(\xi) \sim e^{-\beta\xi}, \qquad \beta > 0. \tag{4.2.4}$$

This leads to a semi–explicit representation of M, obtained by integrating the ECM equation,

$$M(\xi) = \frac{1}{1+\sigma U(\xi)} + \sigma \int_{\xi}^{\infty} \frac{\phi(s)}{(1+\sigma U(s))^2}\frac{dU}{ds}(s)\, ds, \tag{4.2.5}$$

with

$$\phi(s) = \exp\left(-\tfrac{\alpha}{c}\int_{\xi}^{s}(1+\sigma U(\eta))\, d\eta\right). \tag{4.2.6}$$

The details of this derivation are provided in Appendix A.1.
From the semi–explicit representation we can obtain an upper bound for M. Since U decreases monotonically from 1 at $-\infty$ to 0 at $+\infty$, we have $\frac{dU}{d\xi} < 0$ across the front, and therefore

$$0 < M(\xi) \leq \frac{1}{1+\sigma U(\xi)}. \tag{4.2.7}$$

This upper bound is consistent with the structure of equation (4.2.1b), which for fixed U admits the equilibrium value

$$M^* = \frac{1}{1+\sigma U}. \tag{4.2.8}$$

This argument can also be validated with the observation that the dynamics of (4.2.1b) drive M towards the equilibrium M^*, and since U is strictly decreasing $\left(dU/d\xi < 0\right)$, the inequality $M \leq M^*$ is preserved throughout.
Consequently, the effective diffusion function will be simplified to

$$M(1-M) = \frac{\sigma U}{(1+\sigma U)^2}. \tag{4.2.9}$$

In what follows, we restrict attention to the behaviour ahead of the wave, since the analysis behind the front is analogous to the no–source case. We will consider four asymptotic regimes:

- $\sigma \to \infty$: corresponding to strong degradation or weak regeneration,
- $\sigma \to 0$: corresponding to weak degradation or strong regeneration,
- Strong degradation with strong regeneration,
- Weak degradation with weak regeneration.

4.2.1 Strong ratio: $\sigma \to \infty$

With $\sigma \to \infty$, the effective diffusion function (4.2.9) simplifies to

$$M(1-M) = \frac{\sigma U}{(1+\sigma U)^2} \to 0. \tag{4.2.10}$$

Since U also decays exponentially at the leading edge, this does not interfere with the balance and the diffusion contribution vanishes. Consequently, the tumour equation (4.2.1a) reduces to the previously seen (4.1.15) logistic travelling–wave form

$$c\,\frac{dU}{d\xi} + U(1-U) = 0. \tag{4.2.11}$$

As in the no–regeneration case, the solution of this reduced equation automatically satisfies the right (4.1.2a) and left (4.1.2b) boundary conditions consistent with the travelling–wave formulation.

Our simulations, as visible in Figure 4.1, show excellent convergence to the logistic profile (4.2.11) we derived, particularly once α and λ are sufficiently separated in scale, with ratios $\sigma \gtrsim 10^3$ already yielding excellent agreement with the logistic approximation. This confirms that the asymptotic derivation is sufficient to capture the tumour invasion dynamics in these regimes.

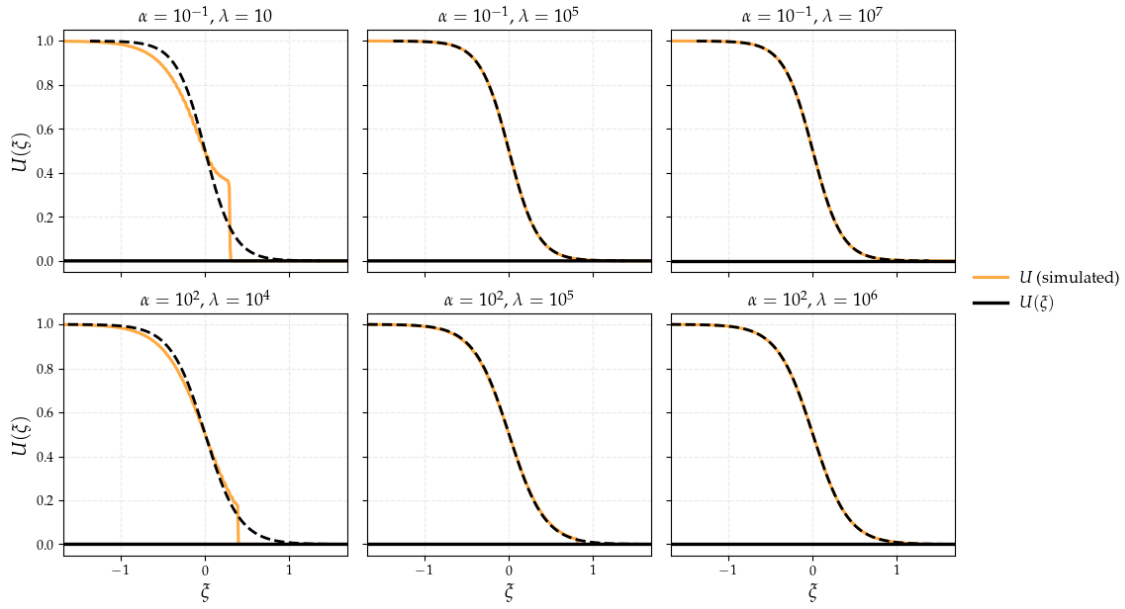

Figure 4.1: Numerical solutions of system (**??**) subject to the initial conditions (2.2.1) and (2.2.2), for $m_0 = 0.5$ and translated into the travelling–wave coordinate ξ. Solid orange lines represent tumour density profiles from numerical simulations, while the dashed black line shows the asymptotic logistic form predicted for $\sigma \to \infty$. In the top row $\alpha = 10^{-1}$ is fixed and $\lambda \in \{10^{-1}, 10^3, 10^6\}$ is varied, while in the bottom row $\alpha = 10^2$ and $\lambda \in \{10^4, 10^5, 10^6\}$

This behaviour is also intuitive, since very weak regeneration ($\alpha \ll 1$) would closely resemble the special case without regeneration, where the ECM is eventually lost, while strong degradation ($\lambda \gg 1$) would overwhelm the benefits of regeneration and degrade any remaining ECM. In both cases the ECM would cease to influence the dynamics, and the only behaviour left would be governed by the tumour population, which survives and spreads through logistic growth driven by competition among cells. The lack of ECM could suggest the tumour struggles to gain movement, becoming restricted to a confined region where invasion is limited to proliferation and competitive interactions, in agreement with the diffusion form of our model.

4.2.2 Weak ratio: $\sigma \to 0$

With $\sigma \to 0$, the effective diffusion function (4.2.9) once again simplifies to

$$\frac{\sigma U}{(1+\sigma U)^2} \to 0. \tag{4.2.12}$$

And we can use the same argument as before to obtain

$$c\,\frac{dU}{d\xi} + U(1-U) = 0. \tag{4.2.13}$$

whose solution automatically satisfies both boundary conditions.

Once again we found a perfect match between the numerical profiles, as seen in Figure B.3, and the logistic prediction (4.2.13) from the asymptotic analysis, just as in the limit $\sigma \to \infty$. This case is particularly interesting because, although the reduced equation is identical to that obtained for $\sigma \to \infty$, the biological interpretation is very different. Here regeneration is very strong ($\alpha \to \infty$) or degradation is very weak ($\lambda \to 0$), so the ECM is continually replenished and effectively saturates the available space, or is scarcely degraded at all. As a result, the tumour cannot advance by breaking down ECM and instead proliferates logistically. In this sense the ECM acts as a physical constraint, forcing invasive competition among tumour cells themselves and limiting spatial spread.

4.2.3 Strong degradation and strong regeneration

We begin by taking equation for the ECM (4.2.1b) and dividing through by α:

$$\frac{c}{\alpha}\,\frac{dM}{d\xi} = 1 - (1+\sigma U)M. \tag{4.2.14}$$

In the regime where both $\lambda \to \infty$ and $\alpha \to \infty$, the ratio $\frac{\lambda}{\alpha} \to 1$ so $\sigma \to 1$. Thus, the ECM relaxes to its equilibrium value

$$M = \frac{1}{1+U} \tag{4.2.15}$$

and provides the diffusion function

$$M(1-M) = \frac{U}{(1+U)^2}. \tag{4.2.16}$$

Substituting this into the tumour equation yields

$$\frac{d}{d\xi}\left(\frac{U}{(1+U)^2}\,\frac{dU}{d\xi}\right) + c\,\frac{dU}{d\xi} + U(1-U) = 0. \tag{4.2.17}$$

The asymptotic profile (4.2.17) departs from the logistic limits from before in forms (4.2.11) and (4.2.13)) and is governed by a nonlinear diffusion equation with coefficient

$$D(U) = \frac{U}{(1+U)^2}. \tag{4.2.18}$$

This arises because the ECM is degraded and replenished at comparable rates, producing a density–dependent diffusion term. Since tumour density is bounded by $U < 1$, the diffusion reaches its maximum value of $1/4$ near saturation. Hence invasion is no longer constrained by too little ECM ($\sigma \to \infty$) or too much ECM ($\sigma \to 0$), but instead produces a travelling wave with a narrow transition zone: the tumour builds up behind the front until it nears carrying capacity, at which point diffusion is strong enough to advance the wave while maintaining a steep drop in density across the interface.

Our simulations confirm this asymptotic structure, but the numerical agreement is less sharp than in the logistic regimes. The fronts follow the predicted profile overall, yet a discrepancy remains in the trailing region behind the wave, and convergence across the parameter sweep is slower. This suggests that interaction with the ECM, which is regenerated about as rapidly as it is degraded, leads to more complex invasion dynamics than those captured by the leading–order asymptotics.

4.2.4 Weak degradation and weak regeneration

Starting from the ECM equation (4.2.1b), in the limit $\alpha \to 0$ it simplifies to

$$c\,\frac{dM}{d\xi} \approx 0, \tag{4.2.19}$$

so that, upon applying the right–hand boundary condition,

$$M(\xi) \approx m_0. \tag{4.2.20}$$

With M constant, the diffusion function becomes

$$M(1-M) \approx m_0(1-m_0), \tag{4.2.21}$$

and, together with $\lambda \to 0$, the tumour travelling–wave equation reduces to the FKPP form

$$m_0(1-m_0)\,\frac{d^2U}{d\xi^2} + c\,\frac{dU}{d\xi} + U(1-U) = 0, \tag{4.2.22}$$

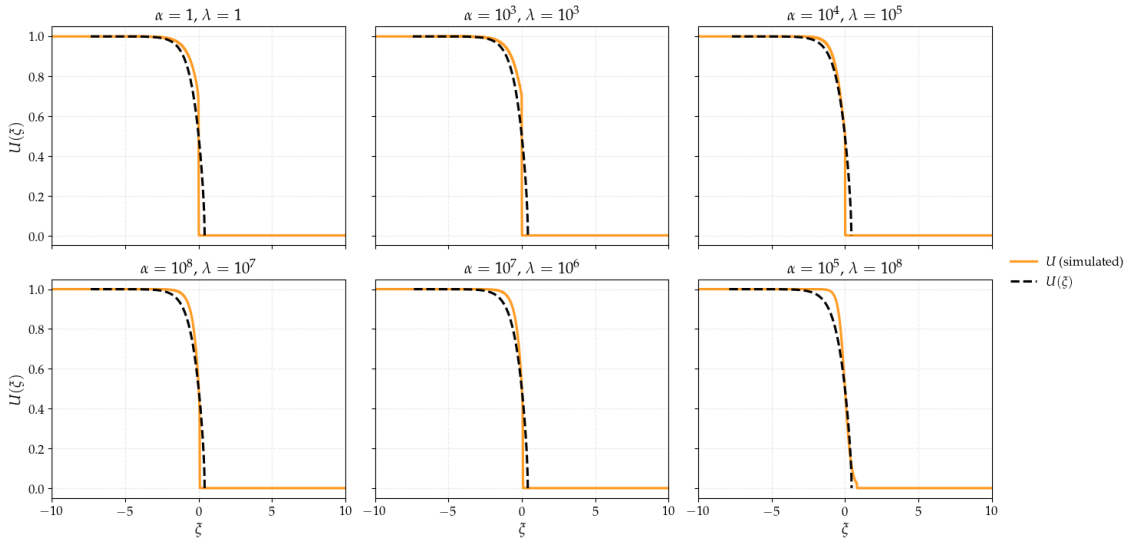

Figure 4.2: Numerical solutions of system (**??**) subject to the initial conditions (2.2.1) and (2.2.2), with initial ECM density fixed at $m_0 = 0.5$ and parameter pairs $(\alpha, \lambda) \in \{(1,1), (10^2, 10^2), (10^4, 10^5), (10^5, 10^7), (10^7, 10^7), (10^7, 10^8)\}$. Solutions are shown in the travelling–wave coordinate ξ defined in (3.1.5), with tumour density $U(\xi)$ from simulations plotted in orange. The asymptotic sharp–front approximation derived from (4.2.17) with boundary conditions (4.1.2) is shown as a dashed black line. The trailing mismatch indicates slower convergence compared to the logistic limits.

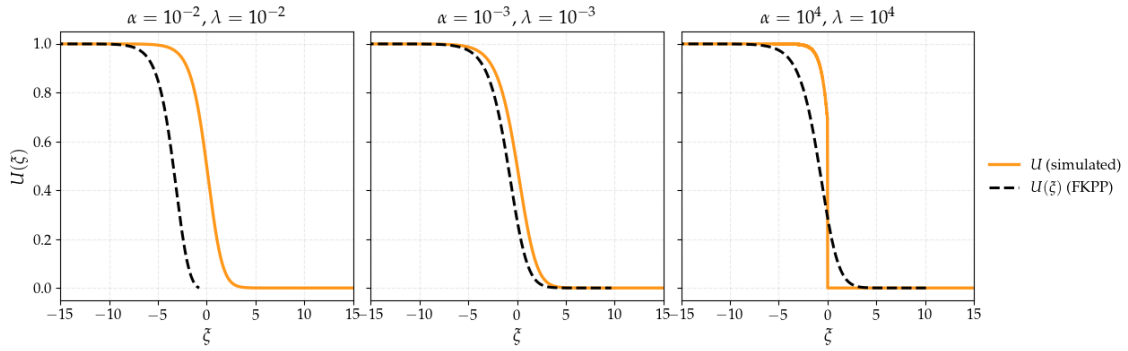

Figure 4.3: Numerical solutions of system (**??**) subject to the initial conditions (2.2.1) and (2.2.2), with initial ECM density fixed at $m_0 = 0.5$ and parameter pairs $(\alpha, \lambda) \in \{(10^{-2}, 10^{-2}), (10^{-3}, 10^{-3}), (10^{5}, 10^{4})\}$. Solutions are translated into the travelling–wave coordinate ξ defined in (**??**), with tumour density $U(\xi)$ from simulations plotted in orange. The asymptotic FKPP profile given by (4.2.22) subject to the boundary conditions (4.1.2) is shown as a dashed black line. The small phase lead indicates slightly faster progression than predicted by the FKPP approximation.

with diffusion $m_0(1 - m_0)$ depending only on the initial amount of ECM.

When both regeneration and degradation are simultaneously weak, the travelling–wave profiles and measured speeds converge towards the FKPP limit predicted by the asymptotics. The simulated fronts, shown in Figure 4.3, are well fitted by the FKPP profile, and the wave speeds are close to the FKPP value. A small but consistent discrepancy remains, however: the numerical front lies slightly ahead of the FKPP prediction, indicating a marginally faster progression that is most visible near the leading edge. Moreover, convergence across the parameter sweep is less sharp than in the logistic limits, suggesting that a correction term beyond the leading–order FKPP approximation is required.

This result is intuitive, since when ECM turnover is negligible, with both degradation and regeneration weak, the ECM remains effectively fixed at its far–field level. The tumour therefore spreads as a FKPP wave, using the initial ECM as a substrate, while the ECM itself is not degraded and continues to occupy space.

Chapter 5

Numerical experiments

In this chapter, we carry out a numerical investigation of the tumour–ECM model to complement the analytical results. The inclusion of nonlinear diffusion and ECM remodelling increases biological realism but reduces analytical tractability. In particular, the travelling–wave analysis classified all fixed points as hyperbolically stable, which was insufficient to determine the existence of connecting trajectories, and a closed–form bound on the minimum wave speed was obtainable only in the absence of regeneration. Numerical methods are therefore employed to address these limitations and to quantify invasion speeds in regimes not accessible to analysis. The no–regeneration case serves as a benchmark against which regeneration scenarios with $\alpha > 0$ are assessed.

5.1 Validation of numerics

We use two complementary numerical approaches. For the PDE model (**??**), we implement a custom finite–difference scheme, as the nonlinear diffusion and coupling in our system require careful treatment to ensure both stability and accuracy [45]. For the ODE system arising from the desingularised TWS (3.2.7), we employ standard adaptive solvers, since these are low–dimensional problems that can be treated efficiently with well–established methods [46].

5.1.1 Scheme selection for PDE

We set the spatial domain of the model to be $[0, L]$. To solve the PDE numerically, this domain is discretised into N equal subintervals, giving a step size $\Delta x =$

L/N and grid points $x_i = i\Delta x$ for $i = 0, \dots, N$. Although the PDE itself has no prescribed finite end time, in practice we simulate up to a fixed horizon T. Time is discretised into uniform steps of size Δt, with $N_t = T/\Delta t$ iterations, giving discrete times $t_j = j\Delta t$ for $j = 0, \dots, N_t$.

The tumour equation has the form of a reaction–diffusion system, which we split into diffusion and reaction parts:

$$u_t = \mathbf{L}(u, m) + \mathbf{N}(u), \tag{5.1.1}$$

where

$$\mathbf{L}(u, m) = \partial_x\big(D\, m(1-m)\, u_x\big), \qquad \mathbf{N}(u) = u(1-u).$$

To discretise $\mathbf{L}$ in space, we use a conservative finite–difference formulation with edge–averaged coefficients. At each half–grid point $x_{i+1/2}$, we set

$$a_{i+1/2} = D\,\overline{m}_{i+1/2}\,\big(1 - \overline{m}_{i+1/2}\big), \qquad \overline{m}_{i+1/2} = \tfrac{1}{2}(m_i + m_{i+1}), \tag{5.1.2}$$

and the resulting discrete operator acting on u is

$$(\mathbf{L}(m)u)_i = \frac{1}{\Delta x^2}\Big[a_{i+1/2}(u_{i+1} - u_i) - a_{i-1/2}(u_i - u_{i-1})\Big]. \tag{5.1.3}$$

At the boundaries we impose homogeneous Neumann conditions, $u_x(0) = u_x(L) = 0$, implemented via ghost points. This yields the modified updates

$$(\mathbf{L}(m)u)_0 = \frac{2}{\Delta x^2}\, a_{1/2}\,(u_1 - u_0), \qquad (\mathbf{L}(m)u)_{N-1} = \frac{2}{\Delta x^2}\, a_{N-1/2}\,(u_{N-2} - u_{N-1}). \tag{5.1.4}$$

The full information on the stencil is available in Appendix B.1.

For stepping forward in time, we choose an Implicit Explicit (IMEX) scheme. These methods allow us to treat diffusion implicitly, ensuring stability, while handling the nonlinear reaction explicitly, preserving efficiency. This splitting is particularly suited to our system, where diffusion can introduce stiffness while the reaction term remains well behaved.

In particular, we adopt the **AB2–AM2 scheme**: Adams–Bashforth of order two for the explicit nonlinear part, and Adams–Moulton of order two for the implicit diffusion part. The discrete update for u is

$$\frac{u^{j+1} - u^j}{\Delta t} = \tfrac{3}{2}\mathbf{N}(u^j) - \tfrac{1}{2}\mathbf{N}(u^{j-1}) + \tfrac{1}{2}\Big[\mathbf{L}(u^{j+1}, m^{j+1}) + \mathbf{L}(u^j, m^j)\Big]. \tag{5.1.5}$$

Compared with other IMEX variants, AB2–AM2 achieves a quadratic rate of convergence and effectively controls error growth in stiff components. This makes

it particularly suitable for fine grids. IMEX schemes are well established in the study of reaction–diffusion systems but remain uncommon in tumour modelling. We adopt this approach because it allows significantly larger time steps whilst still providing stability and good accuracy.

For the ECM equation, we adopt a fully implicit update. Since m has no spatial derivative in the model, its evolution is purely temporal, and we therefore suppress the spatial subscript for clarity. The ECM update is

$$\frac{m^{j+1} - m^j}{\Delta t} = \alpha(1 - m^{j+1}) - \lambda u^{j+1} m^{j+1}, \tag{5.1.6}$$

which has the closed–form solution

$$m^{j+1} = \frac{m^j + \alpha \Delta t}{1 + \Delta t(\alpha + \lambda u^{j+1})}, \tag{5.1.7}$$

with the initial condition $m^0 = m_0$.

We adopt this implicit approach because it remains stable across parameter ranges. By contrast, explicit methods and Crank–Nicolson fail when degradation is large due to stiffness. The implicit scheme permits larger time steps whilst still providing stability and good accuracy, making it particularly well suited to the ECM dynamics.

We avoid traditional alternatives such as explicit Euler or Runge–Kutta methods for our model, as they require very small time steps for stability while achieving the same or worse error. A comparison against such methods is provided in Appendix X, confirming the advantages of the chosen scheme.

Selection of time step and spatial resolution

The accuracy of our scheme was validated against the analytical wave speed for the no–regeneration case, derived from the travelling–wave analysis (3.3.8),

$$c = 2\sqrt{m_0(1 - m_0)}. \tag{5.1.8}$$

We compared numerical results for different initial ECM densities m_0. Figure 5.1 shows the error in computed invasion speeds as the spatial step Δx is refined, for a range of m_0 and degradation rates λ.

The results indicate that the AB2–AM2 scheme converges quadratically, with $\Delta x = 0.01$ sufficient to achieve at least two digits of accuracy in most cases. These

simulations were performed with a relatively large time step $\Delta t = 0.1$, further highlighting the efficiency gained by using AB2–AM2.

It is also observed that accuracy deteriorates for larger initial densities of ECM ($m_0 > 0.5$) and the rate of degradation increases ($\lambda > 10$). Importantly, this loss of accuracy is not a numerical artefact but reflects genuine behaviour of the system, as we shall see in the succeeding sections.

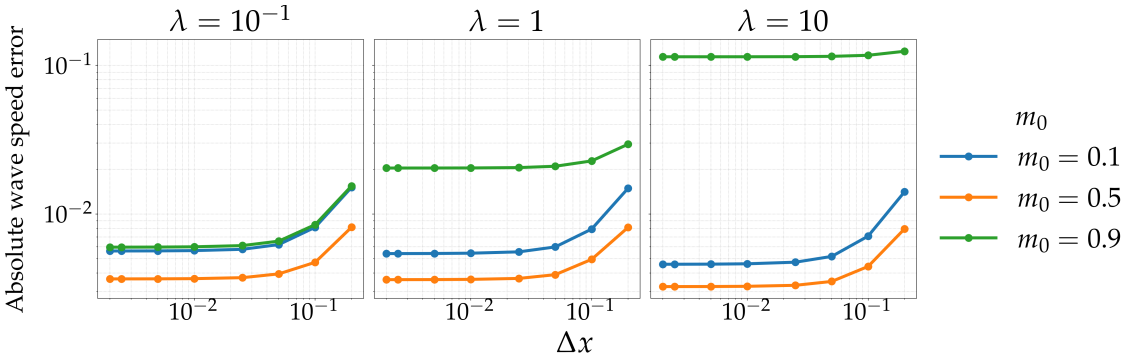

Figure 5.1: Convergence check of the AB2–AM2 scheme for estimating wave speeds in the system (**??**) with initial conditions (2.2.1) and (2.2.2). Simulations were run with domain length $L = 200$, final time $T = 200$, ECM initial densities $m_0 \in \{0.1, 0.5, 0.9\}$, $\alpha = 0$, initial tumour density $u_0 = 1$, and degradation rates $\lambda \in \{0.1, 1, 10\}$. The absolute wave speed error was computed as Error $= \left| c_{\Delta x, \Delta t} - c_{\min} \right|$, where $c_{\Delta x, \Delta t}$ is the numerically estimated wave speed using grid spacings $(\Delta x, \Delta t)$, and $c_{\min} = 2\sqrt{m_0(1 - m_0)}$ is the theoretical minimal speed from the asymptotic analysis. Results show almost quadratic convergence, with $\Delta x = 0.01$ and $\Delta t = 0.1$ sufficient for accurate estimates.

To estimate the tumour front speed, we determined the spatial location at which the wavefront passed a prescribed checkpoint, here set at $u = 0.5$. This crossing point was identified by interpolating the numerical solution in the neighbourhood of the checkpoint. We employed cubic splines from Python's `scipy.interpolate` library [46], which provide an efficient implementation and have been shown to be effective for FKPP-type equations [47].

5.1.2 Scheme selection for ODEs

For the ordinary differential equations arising from the TWS and the desingularised TWS, we employ the standard adaptive RK45 [48]. We follow the same

numerical set-up as in [33], by setting $\tau = 1$ and proceed by using the values of c computed directly from the numerical solution of the PDE system (**??**) with initial conditions (2.2.1) and (2.2.2).

5.2 Analysis of results

5.2.1 No regeneration ($\alpha = 0$)

Effect of amplitude of initial tumour density

The initial condition for the tumour was specified in the form

$$u(x,0) = u_0 \cdot \tfrac{1}{2}\Big[1 - \tanh\big(s(x - p\tilde{L})\big)\Big], \tag{5.2.1}$$

where u_0 is the size of the initial tumour profile. Our travelling–wave analysis indicated that this amplitude does not affect the fixed points of the system. Numerical simulations confirm this finding, as illustrated in Figure B.1, where varying u_0 produces eventually the same invasion speed, $2\sqrt{m_0(1-m_0)}$, in contrast to other parameters which do influence the speed. This shows that variation in u_0 affects only the transient phase, while the long–time dynamics are determined by the system itself. Therefore, we will assume that the tumour is initially saturated, that is $u_0 = 1$.

Effect of initial ECM density

The effect of the initial ECM density m_0 is more substantial. In the no–regeneration case, the closed–form travelling–wave analysis showed that the fixed points of the system depend explicitly on m_0, and that the minimum wave speed is determined solely by this value. This behaviour is visible in the travelling–wave plots of Figure 5.2, where changing m_0 produces distinct patterns of tumour–ECM interaction. Higher values of m_0 lead to a broader region of overlap between tumour and matrix, suggesting that it takes longer for the tumour to degrade through the ECM before advancing.

The corresponding minimum wave speeds are shown in Figure 5.3. The heatmap highlights that the maximum of this speed curve is attained at $m_0 = 0.5$, with slower progression for values of m_0 away from this optimum. The line plots make this dependence clearer: speeds decrease towards both extremes, and the

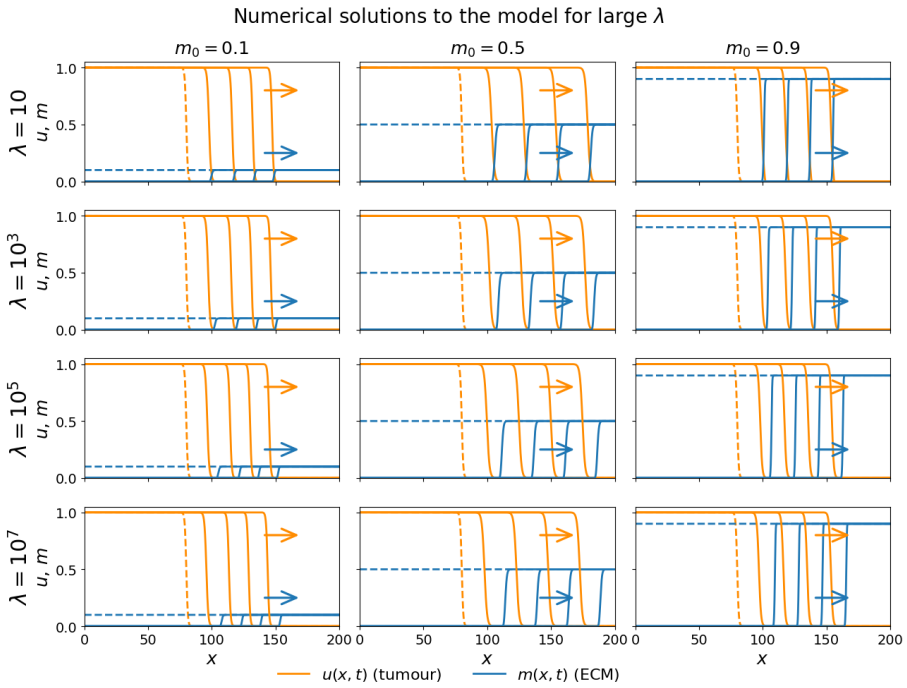

Figure 5.2: Numerical solutions of the system (**??**) subject to the initial conditions (2.2.1) and (2.2.2), for initial ECM densities $m_0 \in \{0.1, 0.5, 0.9\}$ and degradation rates $\lambda \in \{10, 10^3, 10^5, 10^7\}$. Each row corresponds to a fixed value of λ, while each column corresponds to a fixed value of m_0. Tumour cell density u (orange) and ECM density m (blue) are shown at times $t = 0, 25, 50, 75, 100$ (from left to right), with dashed lines indicating the initial conditions. Simulations were performed on the domain $x \in (0, 200)$ up to final time $T = 200$ with initial tumour size $u_0 = 1$. Further specifics of the numerical methods are given in Section 5.1.1.

curve is nearly symmetric about $m_0 = 0.5$, showing that an intermediate amount of ECM is required to achieve the fastest progression. There is, however, a slight disturbance as $m_0 \to 1$, where the reduction in speed is sharper than expected. This effect becomes more apparent for larger values of λ, which suggests that the role of degradation has been underestimated.

Effect of degradation rate

The influence of the degradation rate λ is less substantial than that of the initial ECM density, m_0. In the no–regeneration case, the closed–form expression for the invasion speed depends only on m_0 and does not involve λ, and the simulations

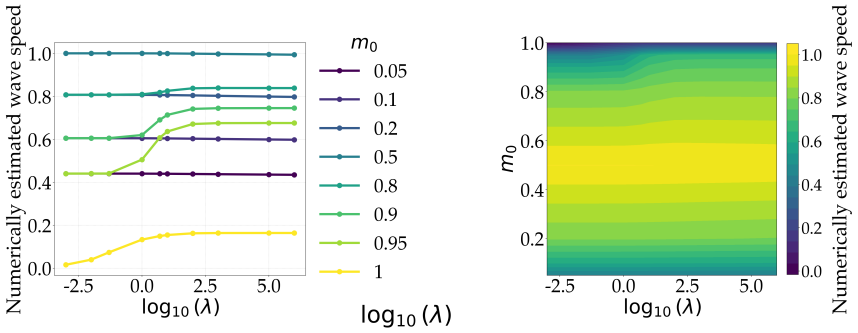

Figure 5.3: Relationship between the numerically estimated minimum wave speeds for travelling–wave solutions of system (**??**) subject to initial conditions (2.2.1) and (2.2.2). Results are shown for $n_0 = 1$ and $m_0 \in \{0.05, 0.1, 0.2, \ldots, 1\}$.

confirm that the speed is unchanged across most values of λ.

An exception arises when $m_0 > 0.5$. In this regime, the invasion speed shows a modest increase once λ exceeds a threshold around 10^2, rising above the closed–form bound but then plateauing. The shift occurs earlier for denser ECM, which also displays the largest proportional increase relative to the bound. Dense ECM therefore slows tumour progression at low λ, but rapid degradation can partly overcome this barrier without fully compensating for it.

This behaviour contrasts with earlier models, which predict convergence across all ECM densities [18, 33]. The threshold–like response observed here suggests that at higher degradation rates, invasion benefits from the presence of additional ECM that can be broken down, effectively providing more substrate for progression. A fuller mechanistic explanation of this effect is required.

5.2.2 Regeneration Source (α)

We now turn to the general model in which ECM regeneration is present. As noted in both the travelling–wave and asymptotic analyses, no closed–form expression for the invasion speed can be obtained in this setting. Our study is therefore based entirely on numerical simulations.

Influence of the initial tumour and ECM distribution

Our analysis showed that, unlike in the absence of regeneration, the initial ECM density no longer determines the long–term invasion speed. With regeneration

present, the system instead undergoes a transition towards saturation that is sustained by the regenerative term, regardless of how low the initial ECM may be. This behaviour can be seen in the travelling–wave profiles of Figure 5.4, where different initial ECM distributions converge, or nearly converge, to similar outcomes once regeneration restores the ECM before the arrival of the tumour.

Influence of the degradation rate (λ)

When the regeneration rate is small, the dependence on λ resembles the behaviour observed in the absence of regeneration. In this regime there is no clear convergence, and the line plots in Figure 5.6 show a slight but persistent increase in invasion speed with increasing λ. Once regeneration becomes moderately significant (around $\alpha \approx 0.1$), the dynamics change qualitatively. A convergence–like behaviour emerges, as seen in Figures 5.5 and 5.6, with invasion speeds stabilising near an upper bound of approximately $c \approx 0.2$. This upper bound is unexpected, since it contrasts with the lower–bound behaviour characteristic of the no–regeneration case reported in the existing literature, and it suggests that regeneration may impose a ceiling on invasion speed. The sharp transition between these two regimes is indicative of a bifurcation, marking the shift from degradation–dominated to regeneration–dominated dynamics.

Influence of the regeneration rate (α)

The novel addition of our model, the regeneration rate, exerts a strong suppressive effect on invasion. Biologically, it works towards healing the system by ensuring that the ECM is replenished prior to tumour arrival, and it continues to act during invasion by counteracting degradation, as illustrated in Figure 5.7. When regeneration is present only at negligible levels, the dynamics resemble those of the absence of regeneration, with degradation dominating the system. However, as α approaches small but significant values, the behaviour changes abruptly: a convergence pattern emerges that nearly arrests tumour progression. Even when degradation rates exceed regeneration, the effect of α remains evident. The invasion speed does not rise beyond the emergent ceiling; instead, the region of maximal progression stabilises around $c \approx 0.2$, as seen in the heatmaps of Figure 5.5. This suggests that regeneration acts as a driver of slower invasion, counteracting degradation and imposing a practical limit on tumour advance.

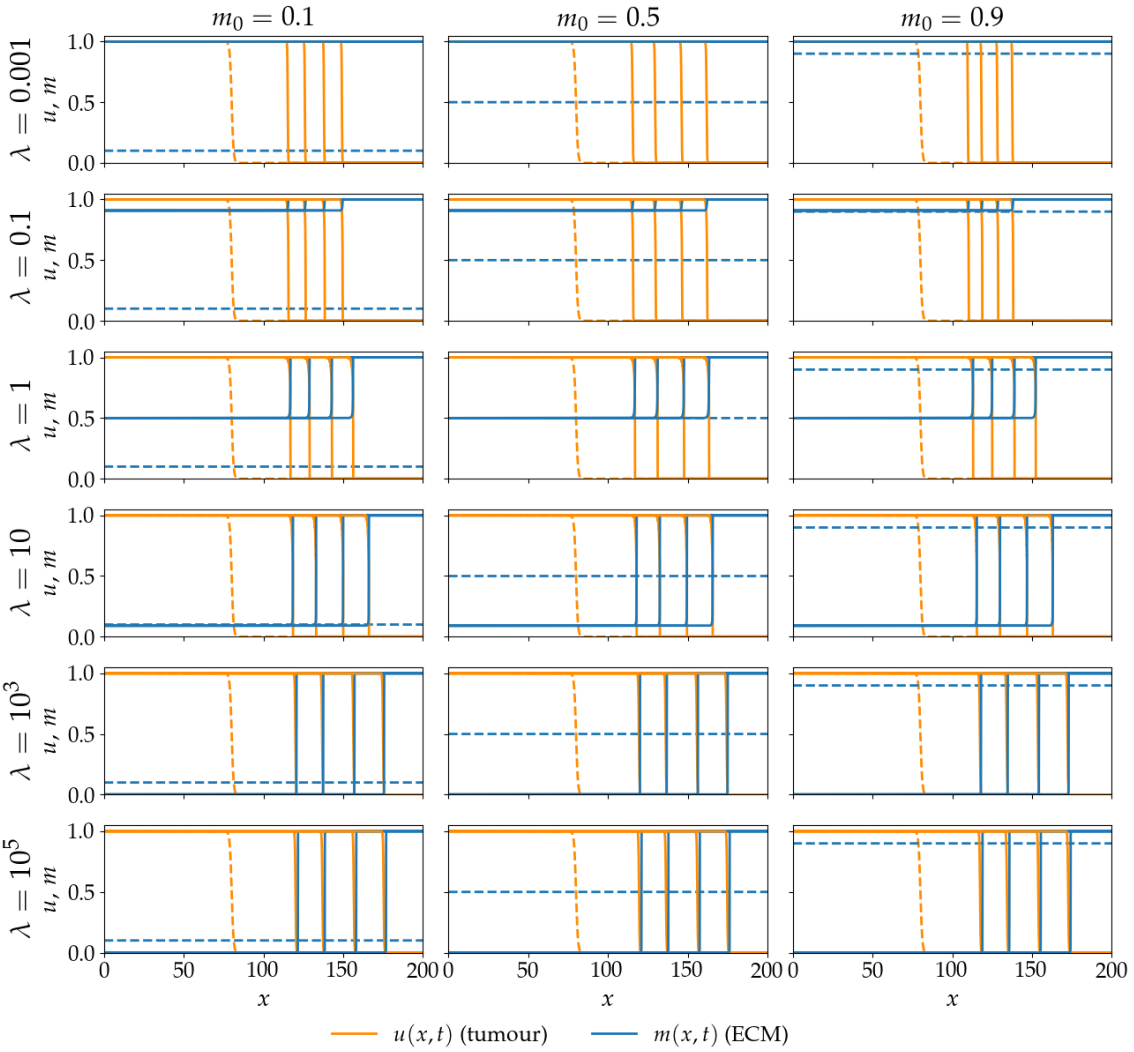

Figure 5.4: Numerical solutions of the system (**??**) subject to the initial conditions (2.2.1) and (2.2.2), with fixed regeneration rate $\alpha = 1$ and initial tumour density $u_0 = 1$. Each column corresponds to a fixed initial ECM density $m_0 \in \{0.1, 0.5, 0.9\}$, while each row corresponds to a fixed degradation rate $\lambda \in \{10^{-3}, 10^{-1}, 1, 10, 10^3, 10^5\}$. Tumour density $u(x,t)$ is shown in orange and ECM density $m(x,t)$ in blue, with dashed lines indicating the initial conditions. Profiles are plotted at times $t = \{0, 100, 200, 300, 400, 500\}$ on the spatial domain $x \in (0, 200)$, with simulations run to a final time $T = 500$, consistent with the conventions described in Section 5.1.1.

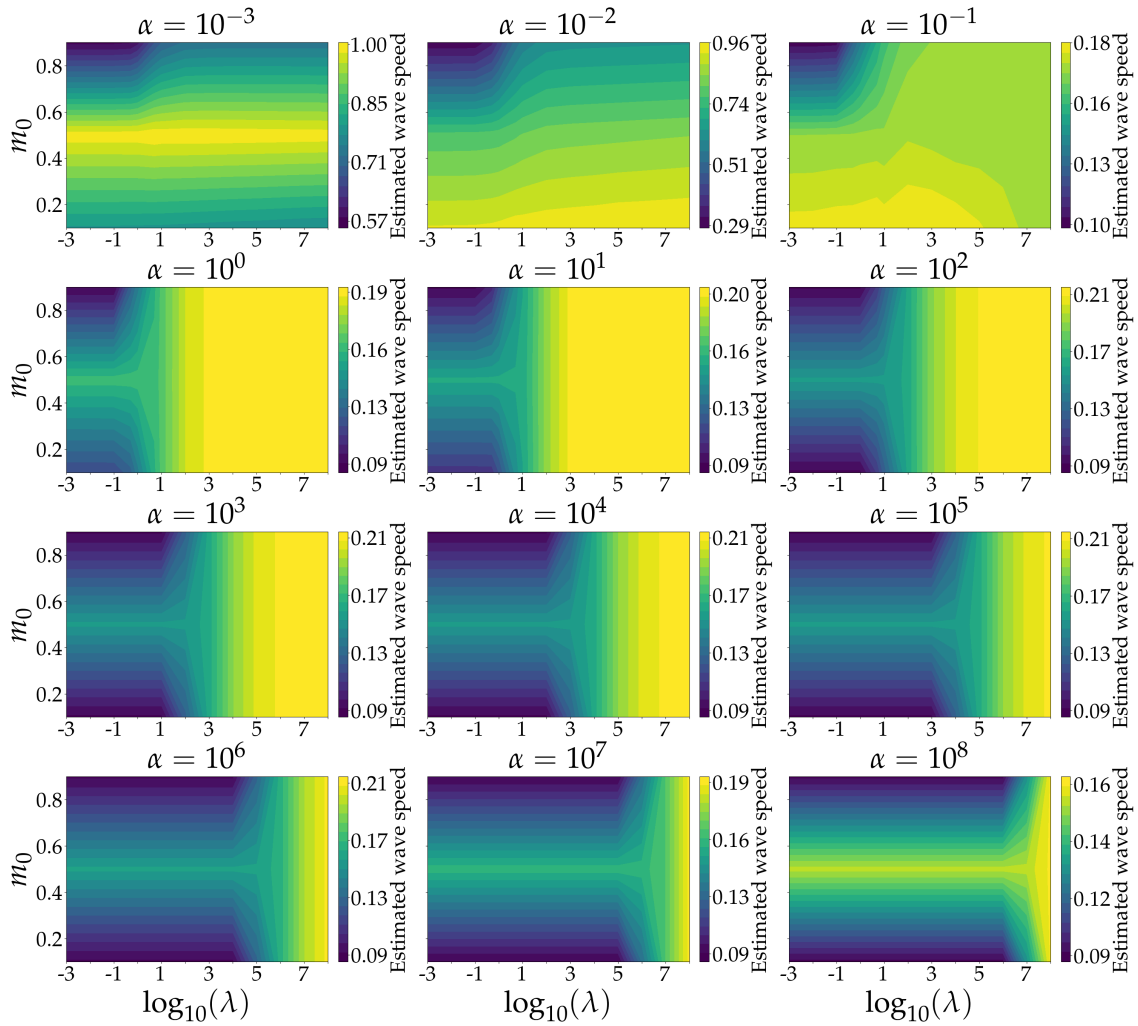

Figure 5.5: Heatmaps of numerically estimated invasion speeds for the system (**??**) subject to the initial conditions (2.2.1) and (2.2.2), with fixed initial tumour density $u_0 = 1$. Each panel corresponds to a fixed value of the regeneration rate $\alpha \in \{10^{-3}, 10^{-2}, \cdots, 10^{6}, 10^{8}\}$, while the horizontal and vertical axes show λ and m_0, respectively. Speeds were estimated numerically by tracking the tumour front $X(t)$ defined by $u(X(t), t) = 0.5$, from simulations on the domain $x \in (0, 200)$ up to final time $T = 500$, following the conventions in Section 5.1.1.

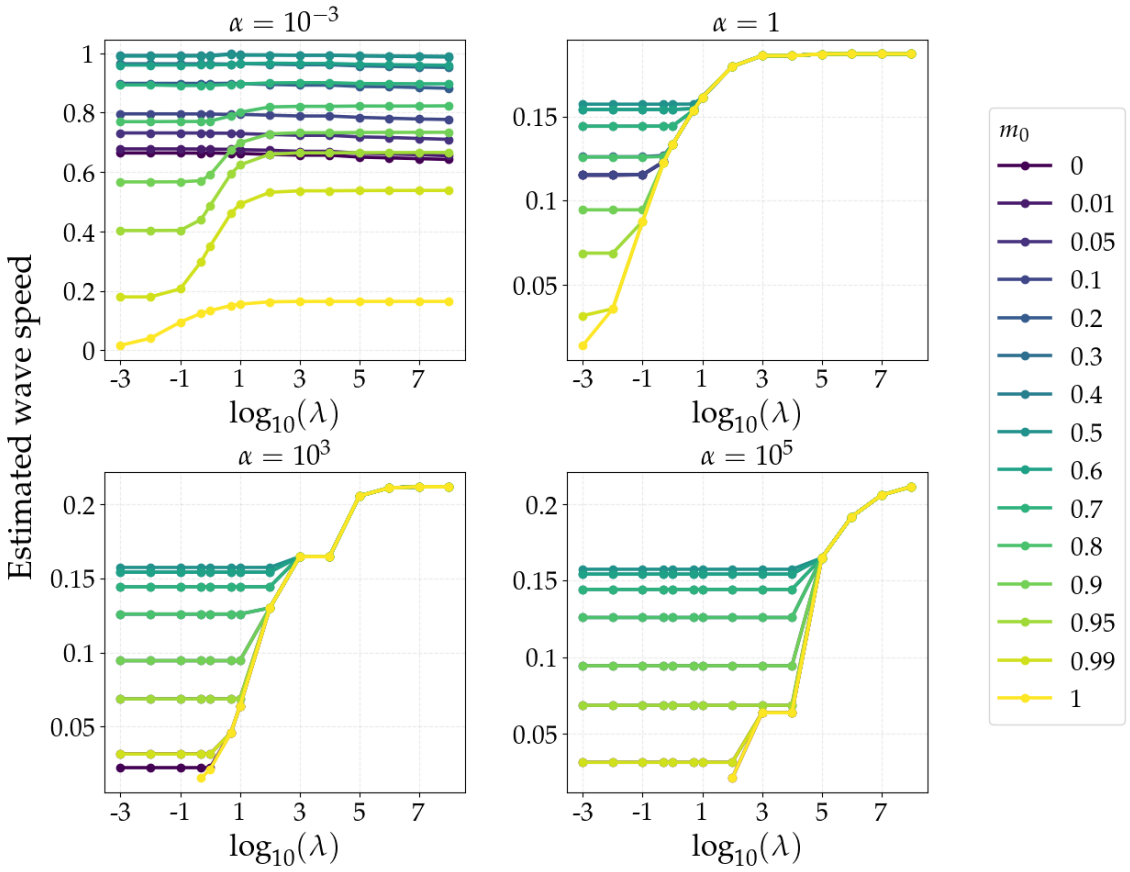

Figure 5.6: Line plots of numerically estimated invasion speeds for $\alpha > 0$. Results correspond to the system (**??**) with initial conditions (2.2.1) and (2.2.2), where the initial tumour density is fixed at $u_0 = 1$. Each panel corresponds to a different regeneration rate, with $\alpha \in \{10^{-3}, 1, 10^3, 10^5\}$. Curves are shown for initial ECM densities $m_0 \in \{0, 0.1, \ldots, 0.99, 1\}$, and degradation rates $\lambda \in \{10^{-3}, 10^{-2}, \ldots, 10^7, 10^8\}$. Wave speeds were numerically estimated by tracking the tumour front $X(t)$, defined by the condition $u(X(t), t) = 0.5$, as described in Section 5.1.1.

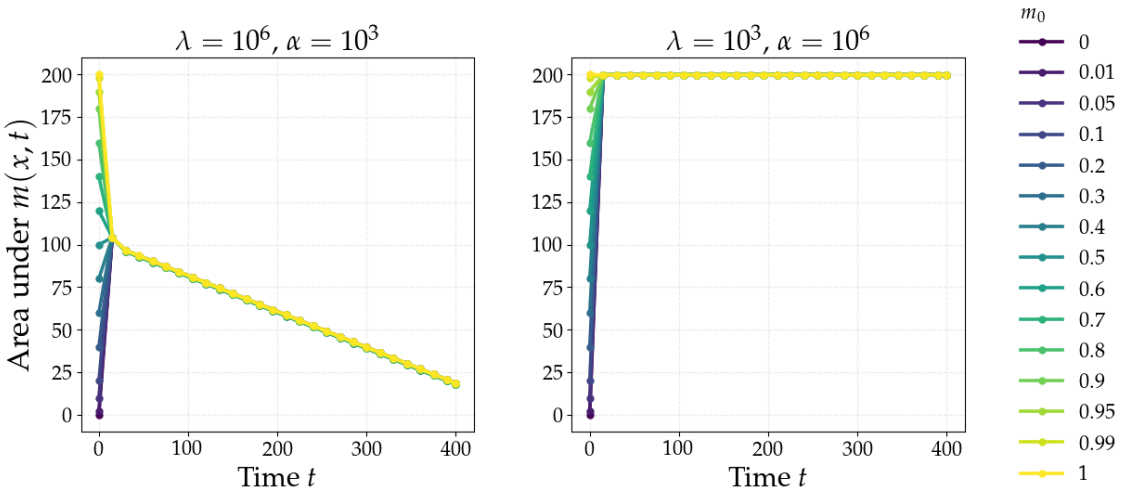

Figure 5.7: Time evolution of the total ECM mass for the system (**??**) subject to the initial conditions (2.2.1) and (2.2.2). The mass was computed as $M(t) = \int_0^{400} m(x,t)\,dx$, with initial tumour density $u_0 = 1$, ECM initial densities $m_0 \in \{0, 0.01, 0.05, \ldots, 1\}$, and parameter values $(\lambda, \alpha) = (10^6, 10^3)$ (left) and $(\lambda, \alpha) = (10^3, 10^6)$ (right). Simulations were run on the domain $x \in (0, 200)$ up to final time $T = 400$, consistent with the conventions described in Section 5.1.1.

Chapter 6

Conclusion and Future Work

In this dissertation, a novel mathematical model of tumour–ECM interactions has been presented and analysed. The formulation introduced two distinctive features. First, tumour motility was modelled through a nonlinear ECM-dependent cross-diffusion term of the form $M(1 - M)$, which reflects the dual role of the ECM in invasion: resisting progression at high density while enabling adhesion and migration when present at intermediate levels. Second, the ECM was endowed with a regeneration mechanism, preventing its density from vanishing entirely and representing the active maintenance of tissue structure.

The analysis combined three complementary approaches: travelling wave analysis, asymptotic analysis, and numerical simulations. While some results aligned with the structure of existing invasion models, the inclusion of both nonlinear diffusion and regeneration produced behaviours that were qualitatively new.

Travelling wave analysis confirmed the existence of invasion fronts and allowed the system to be reformulated in a reduced dynamical setting. A closed-form expression for the wave speed was obtainable only in the special case without regeneration. In this setting, fixed-point analysis revealed an unusual feature: all eigenvalues indicated stability, yet trajectories still connected the equilibria. This behaviour disappeared once regeneration was introduced, underscoring the need for further mathematical investigation to fully understand the underlying stability structure.

Asymptotic analysis was then employed to explore limiting regimes. In certain cases, the dynamics reduced to forms reminiscent of modified FKPP behaviour, particularly under weak degradation. However, new regimes also emerged.

At high degradation or at extreme regeneration rates—both very small and very large—tumour growth simplified to a purely logistic form, independent of ECM dynamics. Moreover, when both degradation and regeneration were simultaneously strong, the system reduced to a tumour-cell-dependent diffusion equation, rather than the ECM-based diffusion of the baseline model. These results highlighted the fundamentally new behaviours generated by the interplay between ECM loss and replenishment.

Numerical simulations provided the third strand of analysis, validating theoretical predictions and probing regimes inaccessible to analysis. In the case of no-regeneration, simulations reproduced the expected behaviour, with wave speeds matching the analytical form at low and moderate ECM densities. Yet a subtle deviation arose at high initial ECM density: when degradation was strong, invasion proceeded slightly faster than predicted, suggesting that an abundance of ECM can, counter-intuitively, facilitate progression. In the regeneration case, numerics revealed a sharp transition. While weak regeneration led to dynamics nearly identical to the no-regeneration model, once the recovery rate surpassed a threshold the invasion speed fell abruptly, resembling a bifurcation. Although not explored in detail here, this observation points to rich and unexplored dynamical structure.

Finally, these findings carry therapeutic implications. Strategies that stimulate ECM recovery—whether through fibroblast activation [49] or enhanced deposition of structural proteins [50, 51, 52]—could contain tumour invasion by reinforcing the surrounding tissue. Such approaches would act in tandem with conventional therapies and highlight the ECM not as a passive barrier but as an actively regulated component of tumour–tissue interactions.

In summary, this work has introduced a new model of tumour–ECM invasion with two innovations: nonlinear ECM-dependent motility and active regeneration. By combining travelling wave reductions, asymptotic methods, and numerical simulations, the study has demonstrated how these mechanisms fundamentally alter invasion dynamics, giving rise to novel regimes and unexpected transitions. The results establish regeneration as a central regulatory mechanism and open new directions for both mathematical investigation and therapeutic exploration.

6.1 Future Work

The model developed in this dissertation represents an initial step toward understanding how ECM availability regulates and constrains tumour invasion. While simplified in several respects, it establishes a framework for exploring the nonlinear interactions between tumour growth, ECM degradation, and tissue-scale processes.

This framework points to several biologically and mathematically rich extensions. Owing to constraints of time, scope, and current biological knowledge, many of these remain unexplored. Nevertheless, several natural directions emerge for future research.

6.1.1 Validation Against Experimental Data

A key limitation of the present work is the absence of validation against experimental or clinical data. Spatial–temporal datasets of tumour expansion and ECM evolution are rare, due to the difficulty of continuously imaging live tissues over extended periods. Without such measurements, quantitative testing of tumour–ECM models remains incomplete. Future progress in imaging, or the construction of surrogate datasets, will be essential to establish biological relevance and allow parameter calibration. Such efforts would enable the refinement of ECM-regulated invasion models and facilitate meaningful comparison with *in vivo* tumour behaviour.

6.1.2 Modelling Directions

The current model allows tumour cells to diffuse nonlinearly, proliferate logistically, degrade ECM, and interact with a regenerating ECM. Several biologically motivated refinements could enhance realism:

(i) Tumour cell death

In the present formulation, logistic growth already enforces cell loss indirectly through crowding, since proliferation vanishes as $u \to 1$. However, tumour cells may also die naturally due to turnover, nutrient deprivation, immune attack, or acidity of the microenvironment. To capture such effects we may add an explicit

linear death term,

$$\frac{\partial u}{\partial t} = \cdots - \delta_u u, \tag{6.1.1}$$

so that cells are removed even in the absence of crowding. This extends the model beyond logistic saturation, and could allow for unique behaviours like extinction of the tumour as mentioned in [53]

(ii) Normal cell populations

The ECM is not only degraded and restored passively but actively maintained by normal stromal or fibroblast cells. Incorporating an additional equation for a normal cell population that regenerates ECM, while competing with the tumour for space and resources, would capture this interplay. Such an addition could provide new insights into how tissue-level homeostasis interacts with tumour invasion.

(iii) ECM remodelling laws

In this work, ECM regeneration was described by a simple linear recovery term. A more realistic representation would allow competition for regenerative capacity. For example,

$$f(u, m) = \alpha(1 - u - m), \tag{6.1.2}$$

models recovery that is suppressed by both tumour and ECM density. Another extension would allow regeneration to diffuse spatially, representing fibroblast-driven ECM production. Similar ideas have been used in wound-healing models and could link tumour dynamics to tissue repair mechanisms [54].

(iv) Tumour proliferation kinetics

A realistic alternative proliferation law is given by Allee-type dynamics [39, 40], where growth is suppressed below a threshold population. In this case one may write

$$f(u) = r\,u\,(u - \theta)(1 - u), \tag{6.1.3}$$

with $\theta \in (0, 1)$ denoting the Allee threshold.

(vi) Matrix metalloproteinases (MMPs)

Our model does not explicitly include the role of MMPs [55]. In reality, tumour cells secrete these proteases, which diffuse through tissue and degrade ECM ahead of the invading front. Incorporating an MMP variable, as in Gatenby–Gawlinski et al [29], would allow our model to capture indirect ECM breakdown and provide a natural link to therapeutic strategies targeting protease activity.

(v) Tumour heterogeneity

The present framework assumes a homogeneous tumour population. In reality, cells may switch between proliferative and migratory phenotypes, as proposed in the "go-or-grow" hypothesis [56]. Applying this principle, as in the work of Crossley et al. [57], within the current framework would clarify how ECM simultaneously acts as both barrier and scaffold.

6.1.3 Mathematical Analysis

Alongside biological extensions, there are several mathematical directions that warrant investigation.

(i) Manifold analysis

The fixed point analysis in this work revealed unusual stability features, with all equilibria stable yet trajectories connecting them in the no-regeneration case. A natural next step is to apply invariant manifold theory to better characterise these structures, providing a clearer understanding of the long-term behaviour of the reduced dynamical system.

(ii) Bifurcation analysis

Numerical simulations revealed an abrupt drop in invasion speed once ECM regeneration surpassed a threshold, resembling a bifurcation. While bifurcation theory is less common in PDE contexts, modern approaches can be applied to investigate this phenomenon. Numerical continuation tools such as `pde2path` [58] provide a framework for tracking solution branches and detecting bifurcation points in discretised PDE systems, while analytical techniques such as weakly nonlinear analysis could be employed to classify the bifurcation type and explore

the stability of emerging solution branches. Such an analysis would provide a deeper understanding of how regeneration fundamentally reshapes invasion dynamics.

6.2 Outlook

This dissertation has shown how tumour–ECM interactions shape invasion dynamics, with regeneration acting as both a barrier and a regulator. By combining travelling–wave analysis, asymptotic methods, and numerical simulations, the work has provided theoretical insight and a framework for further study.

Future progress will require closer integration with data, refinement of biological assumptions, and incorporation of heterogeneity and metastasis. Extending the framework to higher dimensions and complex geometries would allow more realistic comparisons with tissue. Therapeutically, enhancing ECM recovery—through fibroblast activation or pharmacological intervention—could meaningfully alter invasion dynamics, and linking such predictions with experiments would help bridge theory and therapy.

From a mathematical perspective, the study highlights the value of nonlinear diffusion, manifold theory, and bifurcation analysis. Further work is needed to develop these approaches and to fully understand the complex regimes uncovered here, reinforcing the role of applied mathematics in revealing how simple mechanistic rules can generate rich tumour behaviours.

> *"It is not intended to have the last word on the subject, but I hope it may be the first step in a new one."*
> — *Alan Turing, The Chemical Basis of Morphogenesis*, 1952 [1]

Appendices

Appendix A

Supplementary mathematical information

Appendix A: Derivation of the Non-dimensional System

Here we provide the detailed steps showing how the non-dimensional system studied in the main text is obtained from the underlying dimensional equations. This scaling demonstrates how the simplified model can be traced back to biologically interpretable parameters, even though our analysis and numerics are expressed entirely in non-dimensional form.
We begin with the dimensional equations:

$$\frac{\partial u}{\partial t} = \frac{\partial}{\partial x}\left(D\, m\left(1 - \frac{m}{M_x}\right)\frac{\partial u}{\partial x}\right) + r\, u\left(1 - \frac{u}{K}\right), \tag{A.0.1}$$

$$\frac{\partial m}{\partial t} = \tilde{\alpha}\left(1 - \frac{m}{M_x}\right) - \tilde{\lambda}\, u\, m. \tag{A.0.2}$$

Here $u(x,t)$ is tumour cell density, $m(x,t)$ is ECM density, D is the diffusion coefficient, r is the intrinsic tumour growth rate, $K > 0$ is the carrying capacity, and $M_x > 0$ is the maximum ECM density. The dimensional forms of degradation and regeneration are $\tilde{\lambda}$ and and $\tilde{\alpha}$, both of which are nonnegative

To reduce the number of free parameters we introduce the scalings

$$u = K\,\bar{u}, \qquad m = M_x\,\bar{m}, \qquad x = X\,\bar{x}, \qquad t = \rho\,\bar{t}, \tag{A.0.3}$$

where $\bar{u}$ and $\bar{m}$ are non-dimensional tumour and ECM densities, and X and ρ denote characteristic spatial and temporal scales.

Substituting into (A.1.9) gives

$$\frac{K}{\rho}\,\bar{u}_{\bar{t}} = \frac{1}{X}\,\partial_{\bar{x}}\left(DM_x\bar{m}(1-\bar{m})\,\frac{K}{X}\bar{u}_{\bar{x}}\right) + rK\,\bar{u}(1-\bar{u}), \tag{A.0.4}$$

which simplifies to

$$\frac{1}{\rho}\,\bar{u}_{\bar{t}} = \frac{DM_x}{X^2}\,\partial_{\bar{x}}\big(\bar{m}(1-\bar{m})\bar{u}_{\bar{x}}\big) + r\,\bar{u}(1-\bar{u}). \tag{A.0.5}$$

Applying the scalings to (A.1.10) yields

$$\frac{M_x}{\rho}\,\bar{m}_{\bar{t}} = \tilde{\alpha}(1-\bar{m}) - \tilde{\lambda}(K\bar{u})(M_x\bar{m}), \tag{A.0.6}$$

which reduces to

$$\frac{1}{\rho}\,\bar{m}_{\bar{t}} = \frac{\tilde{\alpha}}{M_x}(1-\bar{m}) - \tilde{\lambda}K\,\bar{u}\,\bar{m}. \tag{A.0.7}$$

To balance diffusion and reaction we choose

$$X = \sqrt{\frac{D}{r}}, \qquad \rho = \frac{1}{r}, \tag{A.0.8}$$

so that

$$\frac{DM_x}{X^2} = rM_x, \qquad \frac{1}{\rho} = r. \tag{A.0.9}$$

Introducing the non-dimensional parameters

$$\alpha = \frac{\tilde{\alpha}}{r}, \qquad \lambda = \frac{\tilde{\lambda}K}{r}, \tag{A.0.10}$$

the system becomes

$$\begin{aligned} \bar{u}_{\bar{t}} &= \partial_{\bar{x}}\big(\bar{m}(1-\bar{m})\bar{u}_{\bar{x}}\big) + \bar{u}(1-\bar{u}), \\ \bar{m}_{\bar{t}} &= \alpha(1-\bar{m}) - \lambda\,\bar{u}\,\bar{m}. \end{aligned} \tag{A.0.11}$$

Finally, setting $K = M_x = 1$ and dropping the bars yields the non-dimensional system:

$$\begin{aligned} \frac{\partial U}{\partial T} &= \frac{\partial}{\partial X}\Big(M(1-M)\,\frac{\partial U}{\partial X}\Big) + U(1-U), \\ \frac{\partial M}{\partial T} &= \alpha(1-M) - \lambda UM. \end{aligned} \tag{A.0.12}$$

We emphasise that while the dimensional parameters $(D, r, K, M_x, \tilde{\alpha}, \tilde{\lambda})$ motivate the scaling, our analysis focuses on the non-dimensional parameters α and

λ, together with the initial ECM density m_0 and the initial tumour size. Owing to the novelty of the model structure, there are no experimentally established values for these parameters. Accordingly, they are treated as free variables in this dissertation for the purposes of analysis. The dimensional constants are therefore not assigned explicit values in the main body of the dissertation; their role is solely to justify the reduction to the simplified non-dimensional system analysed here.

Calculation of the Jacobian

The Jacobian of (3.2.7) is defined as

$$J = \frac{\partial(U', P', M')}{\partial(U, P, M)}. \tag{A.0.13}$$

Differentiating term by term gives

$$\begin{array}{lll} \dfrac{\partial U'}{\partial U} = 0, & \dfrac{\partial U'}{\partial P} = 1, & \dfrac{\partial U'}{\partial M} = 0, \\ \dfrac{\partial P'}{\partial U} = -(1-2U)M(1-M), & \dfrac{\partial P'}{\partial P} = -c, & \dfrac{\partial P'}{\partial M} = -(1-U)U(1-2M), \\ \dfrac{\partial M'}{\partial U} = \frac{\lambda}{c}M^2(1-M), & \dfrac{\partial M'}{\partial P} = 0, & \dfrac{\partial M'}{\partial M} = \frac{1}{c}\,b, \end{array}$$

where

$$b = -(3\lambda U + 3\alpha)M^2 + (2\lambda U + 4\alpha)M - \alpha. \tag{A.0.14}$$

Hence the Jacobian takes the compact form

$$J = \begin{pmatrix} 0 & 1 & 0 \\ -(1-2U)M(1-M) & -c & -(1-U)U(1-2M) \\ \frac{\lambda}{c}M^2(1-M) & 0 & \frac{1}{c}\,b \end{pmatrix}. \tag{A.0.15}$$

Fixed points for $\alpha = 0$

Fixed points satisfy $U' = P' = M' = 0$. From (3.2.7a) we obtain $P = 0$. Substituting into (3.2.7b) gives

$$U(1-U)M(1-M) = 0, \tag{A.0.16}$$

so that either $U = 0$, $U = 1$, $M = 0$, or $M = 1$.
For $\alpha = 0$, two relevant equilibria arise:

$$(U, P, M) = (1, 0, 0), \qquad (U, P, M) = (0, 0, \bar{M}), \quad \bar{M} \in (0, 1). \tag{A.0.17}$$

At $(0, 0, \bar{M})$ the Jacobian (A.0.15) reduces to

$$J = \begin{pmatrix} 0 & 1 & 0 \\ -\bar{M}(1-\bar{M}) & -c & 0 \\ 0 & 0 & 0 \end{pmatrix}. \tag{A.0.18}$$

The characteristic polynomial is

$$\det(J - \mu I) = \mu \left(\mu^2 + c\mu + \bar{M}(1-\bar{M}) \right), \tag{A.0.19}$$

so that the eigenvalues are

$$\mu_1 = 0, \qquad \mu_{2,3} = \frac{-c \pm \sqrt{c^2 - 4\bar{M}(1-\bar{M})}}{2}. \tag{A.0.20}$$

The transition between node and spiral behaviour occurs when the discriminant vanishes, i.e.

$$c^2 = 4\bar{M}(1-\bar{M}), \tag{A.0.21}$$

which defines the minimal wave speed

$$c_{\min} = 2\sqrt{\bar{M}(1-\bar{M})}. \tag{A.0.22}$$

At the isolated equilibrium $(U, P, M) = (1, 0, 0)$ the Jacobian reduces to

$$J = \begin{pmatrix} 0 & 1 & 0 \\ 0 & -c & 0 \\ 0 & 0 & 0 \end{pmatrix}, \tag{A.0.23}$$

with eigenvalues

$$\mu_1 = 0, \qquad \mu_2 = 0, \qquad \mu_3 = -c. \tag{A.0.24}$$

Fixed points for $\alpha > 0$

When $\alpha > 0$, the admissible equilibria of (3.2.7) are

$$(U, P, M) = (0, 0, 1), \qquad (U, P, M) = (1, 0, M^*), \quad M^* = \frac{\alpha}{\alpha + \lambda}. \tag{A.0.25}$$

At $(0, 0, 1)$ the Jacobian (A.0.15) has eigenvalues

$$\{0, 0, -c\}. \tag{A.0.26}$$

At $(1, 0, M^*)$, the eigenvalues are

$$\mu_1 = \tfrac{1}{c} b, \qquad \mu_{2,3} = \frac{-c \pm \sqrt{c^2 + 4M^*(1-M^*)}}{2}, \tag{A.0.27}$$

with

$$b = -(3\lambda + 3\alpha)(M^*)^2 + (2\lambda + 4\alpha)M^* - \alpha. \tag{A.0.28}$$

A.1 Derivation for semi-explicit form for asymptotic analysis with regeneration ($\alpha > 0$)

Starting from the travelling–wave equations

$$-c\,\frac{dU}{d\xi} \;+\; \frac{d}{d\xi}\big(M(1-M)\,\frac{dU}{d\xi}\big) \;+\; U(1-U) = 0, \tag{A.1.1a}$$

$$-c\,\frac{dM}{d\xi} \;=\; \alpha(1-M) \;-\; \lambda\,U\,M, \tag{A.1.1b}$$

we introduce the parameter ratio

$$\sigma = \frac{\lambda}{\alpha}. \tag{A.1.2}$$

With this definition, the M–equation (A.1.1b) can be written in the linear form

$$\frac{dM}{d\xi} - \frac{\alpha}{c}\,(1+\sigma U(\xi))\,M = -\,\frac{\alpha}{c}. \tag{A.1.3}$$

Equation (A.1.3) admits the integrating factor

$$\mathcal{I}(\xi) = \exp\!\left(\frac{\alpha}{c}\int_{\xi}^{\infty}\big(1+\sigma U(s)\big)\,ds\right), \tag{A.1.4}$$

chosen so that $\mathcal{I}(+\infty) = 1$. Multiplying (A.1.3) by $\mathcal{I}$ and integrating from ξ to $+\infty$, with the boundary condition $M(+\infty) = 1$, gives

$$M(\xi) = \mathcal{I}(\xi)^{-1}\left[1 + \frac{\alpha}{c}\int_{\xi}^{\infty}\mathcal{I}(s)\,ds\right]. \tag{A.1.5}$$

It is convenient to introduce the instantaneous equilibrium value

$$M^{*}(\xi) = \frac{1}{1+\sigma U(\xi)}, \tag{A.1.6}$$

which satisfies $(\alpha/c)(1+\sigma U)M^{*} = \alpha/c$.
Defining the kernel

$$\phi(\xi,s) = \exp\!\left(-\frac{\alpha}{c}\int_{\xi}^{s}\big(1+\sigma U(\eta)\big)\,d\eta\right), \tag{A.1.7}$$

equation (A.1.5) can be rewritten via an integration–by–parts identity, using

$$\frac{dM^{*}}{ds}(s) = -\,\frac{\sigma\,\frac{dU}{ds}(s)}{(1+\sigma U(s))^{2}},$$

to obtain the semi–explicit representation

$$M(\xi) = \frac{1}{1+\sigma U(\xi)} \;+\; \sigma\int_{\xi}^{\infty}\frac{\phi(\xi,s)\,\frac{dU}{ds}(s)}{(1+\sigma U(s))^{2}}\,ds. \tag{A.1.8}$$

Appendix A: Derivation of the Non-dimensional System

Here we provide the detailed steps showing how the non-dimensional system studied in the main text is obtained from the underlying dimensional equations. This scaling demonstrates how the simplified model can be traced back to biologically interpretable parameters, even though our analysis and numerics are expressed entirely in non-dimensional form.

We begin with the dimensional equations:

$$\frac{\partial u}{\partial t} = \frac{\partial}{\partial x}\left(D\, m\left(1 - \frac{m}{M_x}\right)\frac{\partial u}{\partial x}\right) + r\, u\left(1 - \frac{u}{K}\right), \tag{A.1.9}$$

$$\frac{\partial m}{\partial t} = \tilde{\alpha}\left(1 - \frac{m}{M_x}\right) - \tilde{\lambda}\, u\, m. \tag{A.1.10}$$

Here $u(x,t)$ is tumour cell density, $m(x,t)$ is ECM density, D is the diffusion coefficient, r is the intrinsic tumour growth rate, K is the carrying capacity, and M_x is the maximum ECM density.

To reduce the number of free parameters we introduce the scalings

$$u = K\,\bar{u}, \qquad m = M_x\,\bar{m}, \qquad x = X\,\bar{x}, \qquad t = \rho\,\bar{t}, \tag{A.1.11}$$

where $\bar{u}$ and $\bar{m}$ are non-dimensional tumour and ECM densities, and X and ρ denote characteristic spatial and temporal scales.
Substituting into (A.1.9) gives

$$\frac{K}{\rho}\frac{\partial \bar{u}}{\partial \bar{t}} = \frac{1}{X}\frac{\partial}{\partial \bar{x}}\left(DM_x\bar{m}\,(1-\bar{m})\,\frac{K}{X}\frac{\partial \bar{u}}{\partial \bar{x}}\right) + rK\,\bar{u}\,(1-\bar{u}), \tag{A.1.12}$$

which simplifies to

$$\frac{1}{\rho}\frac{\partial \bar{u}}{\partial \bar{t}} = \frac{DM_x}{X^2}\frac{\partial}{\partial \bar{x}}\left(\bar{m}\,(1-\bar{m})\,\frac{\partial \bar{u}}{\partial \bar{x}}\right) + r\,\bar{u}\,(1-\bar{u}). \tag{A.1.13}$$

Applying the scalings to (A.1.10) yields

$$\frac{M_x}{\rho}\frac{\partial \bar{m}}{\partial \bar{t}} = \tilde{\alpha}\,(1-\bar{m}) - \tilde{\lambda}\,(K\bar{u})(M_x\bar{m}), \tag{A.1.14}$$

which reduces to

$$\frac{1}{\rho}\frac{\partial \bar{m}}{\partial \bar{t}} = \frac{\tilde{\alpha}}{M_x}\,(1-\bar{m}) - \tilde{\lambda}K\,\bar{u}\,\bar{m}. \tag{A.1.15}$$

To balance diffusion and reaction we choose

$$X = \sqrt{\frac{D}{r}}, \qquad \rho = \frac{1}{r}, \tag{A.1.16}$$

so that

$$\frac{DM_x}{X^2} = rM_x, \qquad \frac{1}{\rho} = r. \tag{A.1.17}$$

Introducing the non-dimensional parameters

$$\alpha = \frac{\tilde{\alpha}}{r}, \qquad \lambda = \frac{\tilde{\lambda}K}{r}, \tag{A.1.18}$$

the system becomes

$$\begin{aligned} \frac{\partial \bar{u}}{\partial \bar{t}} &= \frac{\partial}{\partial \bar{x}}\Big(\bar{m}(1-\bar{m})\,\frac{\partial \bar{u}}{\partial \bar{x}}\Big) + \bar{u}(1-\bar{u}), \\ \frac{\partial \bar{m}}{\partial \bar{t}} &= \alpha(1-\bar{m}) - \lambda\,\bar{u}\,\bar{m}. \end{aligned} \tag{A.1.19}$$

Finally, setting $K = M_x = 1$ and dropping the bars yields the non-dimensional system:

$$\begin{aligned} \frac{\partial U}{\partial T} &= \frac{\partial}{\partial X}\Big(M(1-M)\,\frac{\partial U}{\partial X}\Big) + U(1-U), \\ \frac{\partial M}{\partial T} &= \alpha(1-M) - \lambda UM. \end{aligned} \tag{A.1.20}$$

We emphasise that while the dimensional parameters $(D, r, K, M_x, \tilde{\alpha}, \tilde{\lambda})$ motivate the scaling, our analysis focuses on the non-dimensional parameters α and λ, together with the initial ECM density m_0 and the initial tumour size. Owing to the novelty of the model structure, there are no experimentally established values for these parameters. Accordingly, they are treated as free variables in this dissertation for the purposes of analysis. The dimensional constants are therefore not assigned explicit values in the main body of the dissertation; their role is solely to justify the reduction to the simplified non-dimensional system analysed here.

Appendix B

Supplementary information for numerical methods

B.1 Stencil

We discretise the double degenerate cross-diffusion operator using a conservative, finite–volume–style scheme [59] with edge–averaged coefficients, so that fluxes between adjacent nodes cancel exactly. Following the discretisations introduced in 5.1.1, we define

$$M_{i\pm\frac{1}{2}} := \tfrac{1}{2}\,(M_i + M_{i\pm1}),$$

$$a_i := D\,M_{i-\frac{1}{2}}\big(1 - M_{i-\frac{1}{2}}\big),$$

$$b_i := D\,M_{i+\frac{1}{2}}\big(1 - M_{i+\frac{1}{2}}\big).$$

For interior nodes $i = 1, \ldots, N-2$, the stencil takes the form

$$(Lu)_i = \frac{1}{\Delta x^2}\Big[a_i\,(u_{i-1} - u_i) + b_i\,(u_{i+1} - u_i)\Big].$$

At the boundaries we impose homogeneous Neumann conditions

$$u_x(0) = u_x(L) = 0$$

, which leads to the modified first and last rows

$$(Lu)_0 = \frac{2}{\Delta x^2}\,b_0\,(u_1 - u_0), \qquad (Lu)_{N-1} = \frac{2}{\Delta x^2}\,a_{N-1}\,(u_{N-2} - u_{N-1}).$$

Collecting these expressions, the resulting tridiagonal matrix can be written as

$$L = \frac{1}{\Delta x^2}\begin{bmatrix} -2b_0 & 2b_0 & & & \\ a_1 & -(a_1+b_1) & b_1 & & \\ & \ddots & \ddots & \ddots & \\ & & a_{N-2} & -(a_{N-2}+b_{N-2}) & b_{N-2} \\ & & & 2a_{N-1} & -2a_{N-1} \end{bmatrix}.$$

B.2 Effect of amplitude of initial tumour density

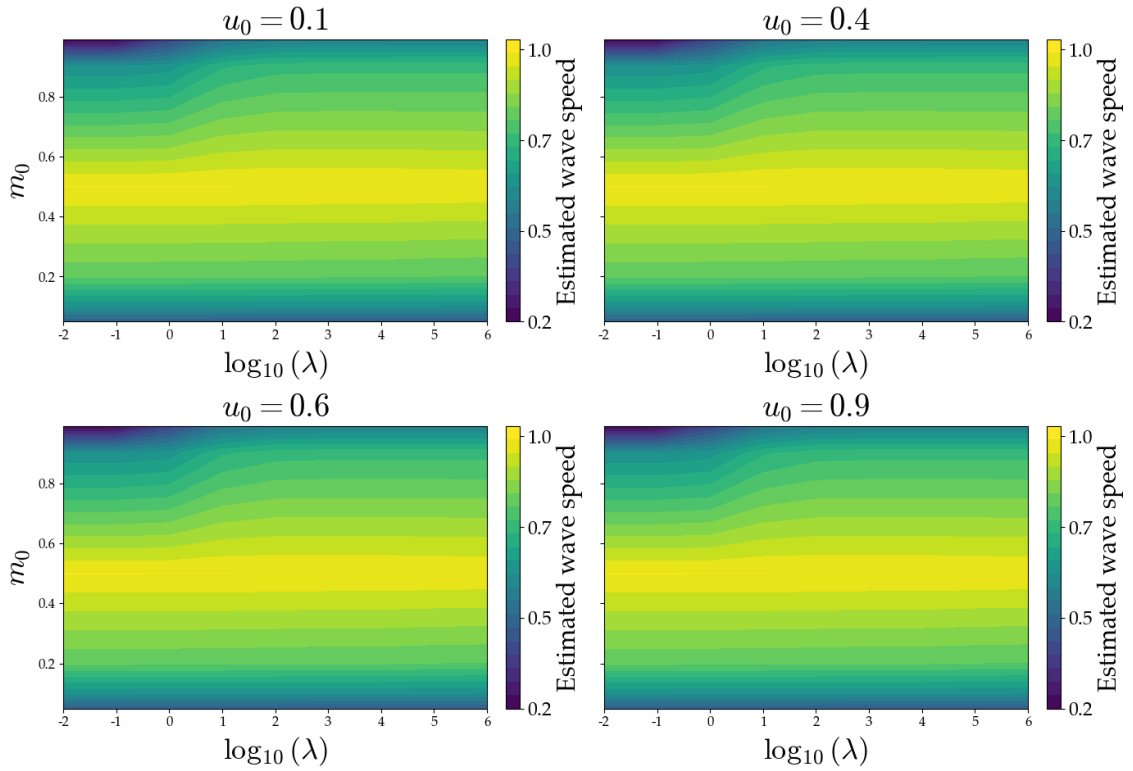

Figure B.1: Heatmaps of numerically estimated invasion speeds for the system (**??**) subject to the initial conditions (2.2.1) and (2.2.2), with no regeneration ($\alpha = 0$). Each panel corresponds to a different initial tumour amplitude, $u_0 \in \{0.1, 0.4, 0.6, 0.9\}$, while the horizontal and vertical axes show λ and m_0, respectively. Speeds were estimated numerically by tracking the tumour front $X(t)$ defined by $u(X(t), t) = 0.5$, from simulations on the domain $x \in (0, 200)$ up to final time $T = 500$, following the conventions in Section 5.1.1.

The initial condition for the tumour was specified in the form

$$u(x, 0) = u_0 \cdot \tfrac{1}{2}\Big[1 - \tanh\big(x - p\tilde{L}\big)\Big], \tag{B.2.1}$$

where u_0 is the size of the initial tumour profile. Our travelling–wave analysis indicated that this amplitude does not affect the fixed points of the system. Numerical simulations confirm this finding, as illustrated in Figure B.1, where varying u_0 produces eventually the same invasion speed, $2\sqrt{m_0(1 - m_0)}$, in contrast to other parameters which do influence the speed. This shows that variation in u_0

affects only the transient phase, while the long–time dynamics are determined by the system itself. Therefore, we will assume that the tumour is initially saturated, that is $u_0 = 1$.

B.3 Parameters used for phase–space projections

The trajectories were computed using SciPy's `solve_ivp` [46] function with the stiff `BDF` method, with `rtol` and `atol` set to 10^{-15} and `max_step` set to 0.01.

Case	m_0	α	λ	**Initial condition (IC)**
No regeneration (Fig. 3.1)	0.2	0	0.1	$(U, P, M) = (0.99, -0.001, 0.20)$
With regeneration (Fig. 3.2)	0.1	0.01	0.1	$(U, P, M) = (0.99, -0.001, 0.1009)$

Table B.1: Parameter sets and initial conditions used for the phase–plane trajectories in Figures 3.1 and 3.2. For the no-regeneration case, the minimal speed is $c_{\text{min}} = 0.80$. For the regeneration case, the measured speed from PDE simulations is $c_{\text{calc}} = 0.7746$ (see Chapter 5).

B.4 Figures from asymptotic analysis

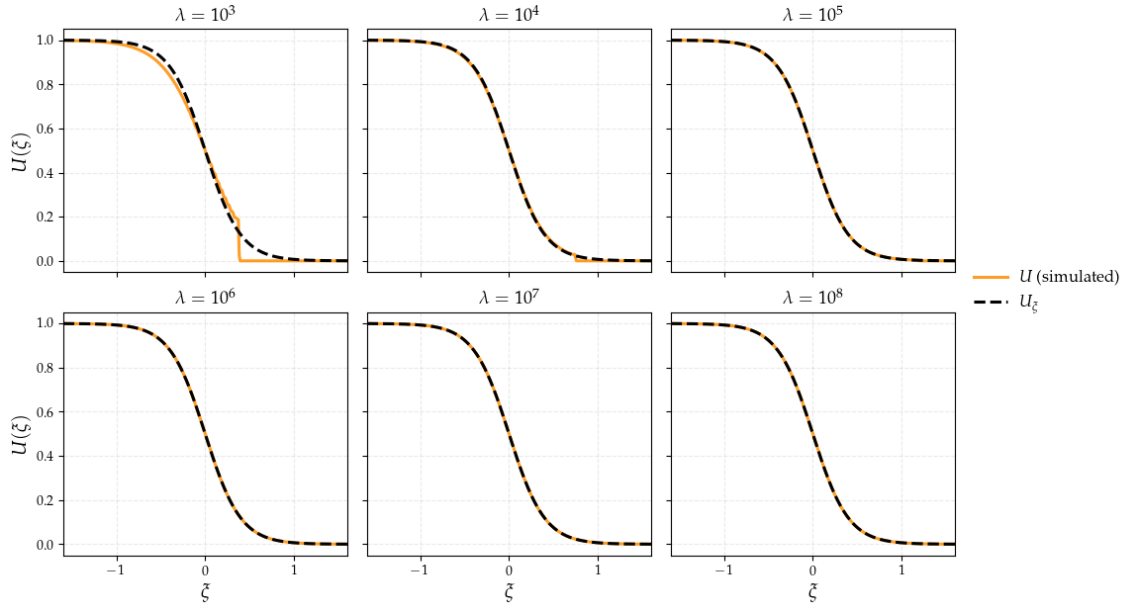

Figure B.2: Numerical solutions of system (**??**) subject to the initial conditions (**??**), for $m_0 = 0.5$ and translated into the travelling–wave coordinate ξ. Solid orange lines represent tumour density profiles from numerical simulations, while the dashed black line shows the asymptotic logistic form. Panels include values of $\lambda = 10^3, \cdots, 10^8$.

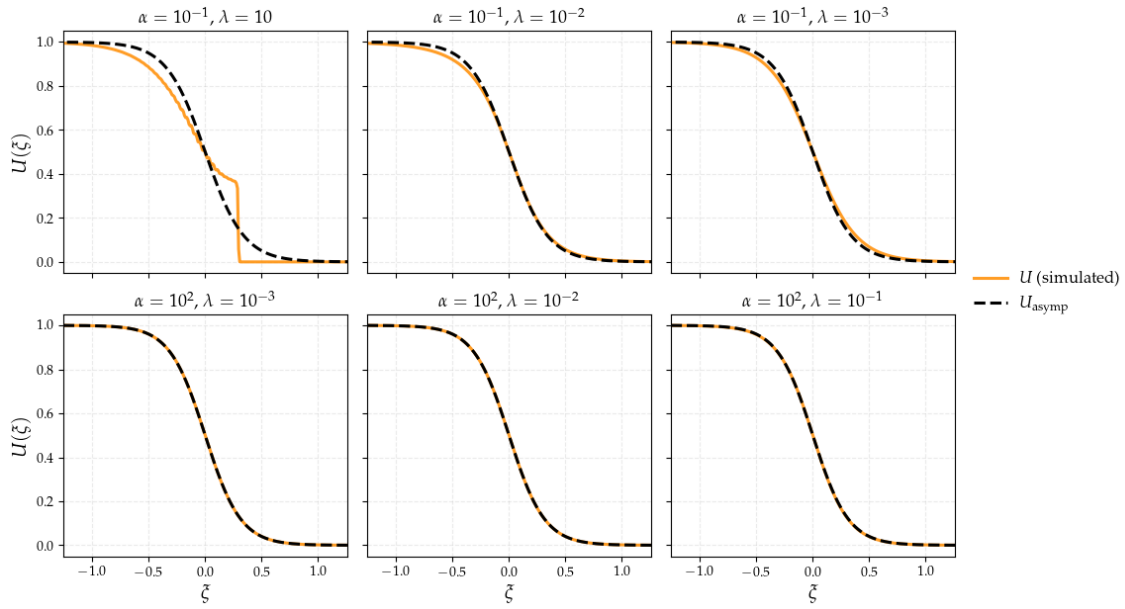

Figure B.3: Numerical solutions of system (**??**) subject to the initial conditions (**??**), for $m_0 = 0.5$ and translated into the travelling–wave coordinate ξ. Solid orange lines represent tumour density profiles from numerical simulations, while the dashed black line shows the asymptotic logistic form. In the top row $\alpha = 10^{-1}$ is fixed and $\lambda \in \{10, 10^{-2}, 10^{-3}\}$ is varied, while in the bottom row $\alpha = 10^{2}$ is fixed and $\lambda \in \{10^{-3}, 10^{-2}, 10^{-1}\}$ is varied.

Appendix C

Supplementary modelling information

C.1 Constant regeneration

We begin with the constant–source formulation

$$u_t \;=\; \partial_x\big(m(1-m)\,u_x\big) + u(1-u), \qquad m_t \;=\; K - \lambda\,u\,m, \tag{C.1.1}$$

with the same nondimensionalisation, initial conditions, and boundary conditions as in Section ().
Introducing the travelling–wave coordinate $\xi = x - ct$ with $n(\xi) = u(x,t)$, the reduced system becomes

$$\frac{d}{d\xi}\big(m(1-m)\,n'\big) + c\,n' + n(1-n) = 0, \qquad c\,m' - \lambda\,n\,m + K = 0. \tag{C.1.2}$$

Upon constructing the Jacobian for this system, we found that the only fixed point consistent with both the PDE and the travelling–wave system is

$$(n, m) = \big(1,\, 0,\, \tfrac{K}{\lambda}\big)\,. \tag{C.1.3}$$

The corresponding eigenvalue calculation shows this state is unstable.

Numerical simulations of the PDE confirm this result: instead of supporting a coherent travelling–wave front, the tumour saturates locally while the ECM grows unbounded due to the constant source term.

C.2 Minimal wave speeds in established invasion models

Model	**Minimal wave speed** $(c_{\min})$	**Notes / Conditions**
Fisher–KPP	2	Classical result from linearisation at the leading edge.
Porous–KPP	$\frac{1}{\sqrt{2}}$	Derived via phase-plane analysis.
Gatenby–Gawlinski	Transcendental equation	Implicit expression; can be solved numerically (e.g. Newton's method [60]).
Colson et al.	$2\sqrt{1-m_0}$	$0 < m_0 < 1$
Browning et al.	$2(1-m_0)$	$0 < m_0 < 1$
	0	$m_0 = 1$ and $\lambda \to 0$
	2^-	$\lambda \to \infty$
Crossley et al.	$2(1-m_0)$	$\lambda \to 0$
	2^-	$\lambda \to \infty$

Table C.1: Summary of minimal wave speeds in selected invasion models.

Bibliography

[1] A. M. Turing. The chemical basis of morphogenesis. *Philos. Trans. R. Soc. Lond. B*, 237(641):37–72, 1952.

[2] M. Xue and C. J. Jackson. Extracellular matrix reorganization during wound healing and its impact on abnormal scarring. *Adv. Wound Care*, 4(3):119–136, 2015.

[3] E. Henke, R. Nandigama, and S. Ergün. Extracellular matrix in the tumor microenvironment and its impact on cancer therapy. *Front. Mol. Biosci.*, 6:160, 2020.

[4] J. R. Todd, K. A. Ryall, S. Vyse, J. P. Wong, R. C. Natrajan, Y. Yuan, A.-C. Tan, and P. H. Huang. Systematic analysis of tumour cell–extracellular matrix adhesion identifies independent prognostic factors in breast cancer. *Oncotarget*, 7(43):71345–71360, 2016.

[5] Cancer Research UK. Lifetime risk of cancer, 2025.

[6] R. L. Siegel, K. D. Miller, N. S. Wagle, and A. Jemal. Cancer statistics, 2024. *CA Cancer J. Clin.*, 74(1):5–28, 2024.

[7] Emily C. S. Scott and Peter J. Hoskin. Health inequalities in cancer care: a literature review of pathways to diagnosis in the united kingdom. *eClinicalMedicine*, 2024.

[8] G. W. Prager, S. Braga, B. Bystricky, C. Qvortrup, C. Criscitiello, E. Esin, G. S. Sonke, G. Argilés Martínez, J.-S. Frenel, M. Karamouzis, M. Strijbos, O. Yazici, P. Bossi, S. Banerjee, T. Troiani, A. Eniu, F. Ciardiello, J. Tabernero, C. C. Zielinski, P. G. Casali, F. Cardoso, J.-Y. Douillard, S. Jezdic, K. McGregor, G. Bricalli, M. Vyas, and A. Ilbawi. Global cancer control: Responding

to the growing burden, rising costs and inequalities in access. *ESMO Open*, 3(2):e000285, 2018.

[9] A. I. Riggio, M.-L. Perrin, Y. Vaggi, and C. Swanton. The lingering mysteries of metastatic recurrence in breast cancer. *British Journal of Cancer*, 2021.

[10] S. U. Khan, M. Khalid, S. Kausar, A. Zafar, and Z. A. Khan. Unveiling the mechanisms of cancer progression: recurrence, dormancy, and drug resistance. *Cell Communication and Signaling*, 2024.

[11] Z. N. Lei, X. P. Li, L. Liu, and Y. Cao. Understanding and targeting resistance mechanisms in cancer therapy. *Signal Transduction and Targeted Therapy*, 2023.

[12] Q. Liu, H. Zhang, X. Jiang, C. Qian, Z. Liu, and D. Luo. Factors involved in cancer metastasis: a better understanding to "seed and soil" hypothesis. *Molecular Cancer*, 2017.

[13] G. Arumugam and J. Tyagi. Keller–Segel chemotaxis models: a review. *Acta Appl. Math.*, 2021.

[14] K. J. Painter. Mathematical models for chemotaxis and their applications in self-organisation phenomena. *J. Theor. Biol.*, 457:165–187, 2019.

[15] V. Cristini, X. Li, J. S. Lowengrub, and S. M. Wise. Nonlinear simulations of solid tumour growth using a mixture model: invasion and branching. *J. Math. Biol.*, 58(4–5):723–763, 2009.

[16] H. Helisaz, M. H. Saidi, and A. Sadeghi. 3d modelling of reaction–diffusion dynamics in an electrokinetic y-shaped microreactor. *Sens. Actuators B Chem.*, 232:618–627, 2016.

[17] R. A. Fisher. The wave of advance of advantageous genes. *Ann. Eugen.*, 7(4):355–369, 1937.

[18] M. El-Hachem, S. W. McCue, and M. J. Simpson. Travelling wave analysis of cellular invasion into surrounding tissues. *Physica D*, 424:133026, 2021.

[19] C. Colson, F. Sánchez-Garduño, H. M. Byrne, P. K. Maini, and T. Lorenzi. Travelling-wave analysis of a model of tumour invasion with degenerate, cross-dependent diffusion. *Proc. R. Soc. A*, 477(2251):20210593, 2021.

[20] M. J. Ablowitz and A. Zeppetella. Explicit solutions of fisher's equation for a special wave speed. *Bulletin of Mathematical Biology*, 1979.

[21] G. C. Paul, T. Tauhida, and D. Kumar. Revisiting Fisher–KPP model to interpret the spatial spreading of invasive cell population in biology. *Heliyon*, 8(10):e10773, 2022.

[22] A. Habbal, H. Barelli, and G. Malandain. Assessing the ability of the 2d Fisher–KPP equation to model cell-sheet wound closure. *Math. Biosci.*, 252:33–46, 2014.

[23] G. Cantin, A. Ducrot, and B. M. Funatsu. Mathematical modeling of forest ecosystems by a reaction–diffusion–advection system: impacts of climate change and deforestation. *J. Math. Biol.*, 83(6–7):66, 2021.

[24] J. D. Murray. *Mathematical Biology I: An Introduction*. Springer, 2001.

[25] M. J. Simpson and S. W. McCue. Fisher–KPP-type models of biological invasion: Open source computational tools, key concepts and analysis. *Proc. R. Soc. A*, 2024.

[26] Y. Du and Z. Guo. The stefan problem for the fisher–KPP equation. *J. Differ. Equ.*, 253(4):996–1036, 2012.

[27] N. T. Fadai and M. J. Simpson. New travelling wave solutions of the porous–fisher model with a moving boundary, 2019.

[28] Y. Du and Z. Guo. Spreading–vanishing dichotomy in a diffusive logistic model with a free boundary, ii. *J. Differ. Equ.*, 250(12):4336–4366, 2011.

[29] R. A. Gatenby and E. T. Gawlinski. A reaction–diffusion model of cancer invasion. *Cancer Res.*, 56(24):5745–5753, 1996.

[30] M. V. Liberti and J. W. Locasale. The Warburg effect: How does it benefit cancer cells? *Trends Biochem. Sci.*, 41(3):211–218, 2016.

[31] A. P. Browning, P. Haridas, and M. J. Simpson. A bayesian sequential learning framework to parameterise continuum models of melanoma invasion into human skin. *Bull. Math. Biol.*, 81:676–697, 2019.

[32] K. Chauhan, D. K. Ebner, K. Tzou, K. Ryan, J. May, T. Kaleem, D. Miller, W. Stross, T. D. Malouff, R. Landy, G. Strong, S. Herchko, C. Serago, D. M. Trifiletti, R. C. Miller, S. Buskirk, and M. R. Waddle. Assessment of bladder filling during prostate cancer radiation therapy with ultrasound and cone-beam ct. *Frontiers in Oncology*, 2023.

[33] R. M. Crossley, P. K. Maini, T. Lorenzi, and R. E. Baker. Travelling waves in a coarse-grained model of volume-filling cell invasion: Simulations and comparisons, 2023.

[34] G. M. Cooper. *The Cell: A Molecular Approach*. Sinauer Associates, Sunderland, MA, 2 edition, 2000.

[35] B. Alberts, A. Johnson, J. Lewis, and et al. *Molecular Biology of the Cell*. Garland Science, New York, 4 edition, 2002.

[36] R. Levayer. Solid stress, competition for space and cancer: The opposing roles of mechanical cell competition in tumour initiation and growth. *Semin. Cancer Biol.*, 63:69–80, 2020.

[37] L. Wagstaff, G. Kolahgar, and E. Piddini. Competitive cell interactions in cancer: a cellular tug of war. *Int. J. Biochem. Cell Biol.*, 23(4):160–167, 2013.

[38] A. Brú, S. Albertos, J. L. Subiza, J. L. García-Asenjo, and I. Brú. The universal dynamics of tumor growth. *Biophys. J.*, 85(5):2948–2961, 2003.

[39] K. Böttger, H. Hatzikirou, A. Voss-Böhme, E. A. Cavalcanti-Adam, M. A. Herrero, and A. Deutsch. An emerging allee effect is critical for tumor initiation and persistence. *PLoS Comput. Biol.*, 11(9):e1004366, 2015.

[40] K. E. Johnson, G. Howard, W. Mo, M. K. Strasser, E. A. B. F. Lima, S. Huang, and A. Brock. Cancer cell population growth kinetics at low densities deviate from the exponential growth model and suggest an allee effect. *PLoS Biol.*, 17(8):e3000399, 2019.

[41] A. Tafech and A. Stéphanou. On the importance of acidity in cancer cells and therapy. *Biology*, 13(4):225, 2024.

[42] M. Marozzi, A. Parnigoni, A. Negri, M. Viola, D. Vigetti, A. Passi, E. Karousou, and F. Rizzi. Inflammation, extracellular matrix remodeling, and proteostasis in tumor microenvironment. *Cancers*, 13(15):3690, 2021.

[43] X. Wang, S. Yu, L. Xie, M. Xiang, and H. Ma. The role of the extracellular matrix in cardiac regeneration. *Heliyon*, 11(1):e41157, 2025.

[44] W. Liu. Decay rates of energy of the 1d damped original nonlinear wave equation. *Nonlinear Anal. Real World Appl.*, 61:103412, 2021.

[45] E. Hairer and G. Wanner. *Solving Ordinary Differential Equations II: Stiff and Differential-Algebraic Problems*. Springer Series in Computational Mathematics. Springer, 1996.

[46] P. Virtanen, R. Gommers, T. E. Oliphant, M. Haberland, T. Reddy, D. Cournapeau, E. Burovski, P. Peterson, W. Weckesser, J. Bright, S. J. van der Walt, M. Brett, J. Wilson, K. J. Millman, N. Mayorov, A. R. J. Nelson, E. Jones, R. Kern, E. Larson, C. J. Carey, İ. Polat, Y. Feng, E. W. Moore, J. VanderPlas, D. Laxalde, J. Perktold, R. Cimrman, I. Henriksen, E. A. Quintero, C. R. Harris, A. M. Archibald, A. H. Ribeiro, F. Pedregosa, and P. van Mulbregt. Scipy 1.0: fundamental algorithms for scientific computing in python. *Nat. Methods*, 17:261–272, 2020.

[47] C. de Boor. *A Practical Guide to Splines*. Springer, 2001.

[48] E. Fehlberg. Low-order classical Runge–Kutta formulas with step size control and their application to some heat transfer problems. *NASA Tech. Rep.*, (R-315), 1969.

[49] L. E. Tracy, R. A. Minasian, and E. J. Caterson. Extracellular matrix and dermal fibroblast function in the healing wound. *Adv. Wound Care*, 5(3):119–136, 2016.

[50] J. J. Lee, K. Y. Ng, and A. Bakhtiar. Extracellular matrix: unlocking new avenues in cancer treatment. *Biomark. Res.*, 13(1):38, 2025.

[51] F. A. Venning, L. Wullkopf, and J. T. Erler. Targeting ECM disrupts cancer progression. *Front. Oncol.*, 5:224, 2015.

[52] X. Feng, F. Cao, X. Wu, W. Xie, P. Wang, and H. Jiang. Targeting extracellular matrix stiffness for cancer therapy. *Front. Immunol.*, 15:1467602, 2024.

[53] Natasha K. Martin, Eamonn A. Gaffney, Robert A. Gatenby, and Philip K. Maini. Tumour–stromal interactions in acid-mediated invasion: A mathematical model. *Journal of Theoretical Biology*, 2010.

[54] P. Lu, K. Takai, V. M. Weaver, and Z. Werb. Extracellular matrix degradation and remodeling in development and disease. *Cold Spring Harb. Perspect. Biol.*, 3(12):a005058, 2011.

[55] M. Egeblad and Z. Werb. New functions for the matrix metalloproteinases in cancer progression. *Nat. Rev. Cancer*, 2002.

[56] A. Tursynkozha, D. C. Harris, Y. Kuang, and A. Kashkynbayev. Go-or-grow-or-die as a framework for the mathematical modeling of glioblastoma dynamics. *Math. Biosci.*, 374:109520, 2025.

[57] R. M. Crossley, K. J. Painter, T. Lorenzi, P. K. Maini, and R. E. Baker. Phenotypic switching mechanisms determine the structure of cell migration into extracellular matrix under the 'go-or-grow' hypothesis. *Math. Biosci.*, 370:109240, 2024.

[58] H. Uecker, D. Wetzel, and J. D. M. Rademacher. pde2path: A matlab package for continuation and bifurcation in 2d elliptic systems. *arXiv preprint arXiv:1208.3112*, 2012.

[59] D. Lobo. Fast stable finite difference schemes for nonlinear cross-diffusion. *arXiv preprint arXiv:2105.04043*, 2021.

[60] Richard A. Holmgren. *A First Course in Discrete Dynamical Systems*. Universitext. Springer, 2000.